Unraveling late Quaternary atmospheric circulation in the Southern Hemisphere through the provenance of Pampean loess

Gabriela Torre, Diego Gaiero, Renata Coppo, Nicolás Cosentino, Steven Goldstein, François de Vleeschouwer, Gaël Le Roux, Louise Bolge, Yael Kiro, André Oliveira Sawakuchi

Unraveling late Quaternary atmospheric circulation in the Southern Hemisphere through the provenance of Pampean loess

Article *in* Earth-Science Reviews · September 2022

DOI: 10.1016/j.earscirev.2022.104143

CITATIONS
0

READS
162

10 authors, including:

Gabriela Torre
National University of Cordoba, Argentina
15 PUBLICATIONS **52** CITATIONS
SEE PROFILE

Diego M Gaiero
National University of Cordoba, Argentina
75 PUBLICATIONS **2,402** CITATIONS
SEE PROFILE

Renata Coppo
Centro de Investigaciones en Ciencias de la Tierra
13 PUBLICATIONS **47** CITATIONS
SEE PROFILE

Nicolás J. Cosentino
Pontificia Universidad Católica de Chile
39 PUBLICATIONS **199** CITATIONS
SEE PROFILE

Unraveling late Quaternary atmospheric circulation in the Southern Hemisphere through the provenance of Pampean loess

Gabriela Torre[a,b], Diego Gaiero[a,b], Renata Coppo[a,b], Nicolás J. Cosentino[c], Steven L. Goldstein[d,e], François De Vleeschouwer[f], Gael Le Roux[g], Louise Bolge[d], Yael Kiro[d], André Oliveira Sawakuchi[h]

[a] Universidad Nacional de Córdoba, Facultad de Ciencias Exactas, Físicas y Naturales. Av. Vélez Sarsfield 299, X5000JJC Córdoba, Argentina

[b] Consejo Nacional de Investigaciones Científicas y Tecnológicas (CONICET), Centro de Investigaciones en Ciencias de la Tierra (CICTERRA), Av. Vélez Sarsfield 1611, Edificio CICTERRA, X5016GCA, Ciudad Universitaria, Córdoba, Argentina

[c]Instituto de Geografía, Facultad de Historia, Geografía y Ciencia Política, Pontificia Universidad Católica de Chile

[d] Lamont-Doherty Earth Observatory, Columbia University, 61 Route 9W, Palisades, NY 10964, USA

[e] Department of Earth and Environmental Sciences, Columbia University, New York, NY, 10025 USA

[f]Instituto Franco-Argentino para el Estudio del Clima y sus Impactos (UMI IFAECI/CNRS-CONICET-UBA-IRD), Ciudad Autónoma de Buenos Aires, Argentina.

[g]Laboratoire Ecologie Fonctionnelle et Environnement, Université de Toulouse, CNRS, Toulouse, France

[h]Instituto de Geociências, Universidade de São Paulo, Rua do Lago, 562, SP, São Paulo, 05508-080, Brazil

Corresponding author: gabrielatorre@unc.edu.ar

Abstract

The Pampean loess is the most extensive continental paleo-record of aeolian material in the Southern Hemisphere, recording the deposition of dust transported by two major zonal wind systems: the southern westerly winds and the subtropical jets. In order to increase the

understanding on paleo-atmospheric circulation over the Southern Hemisphere, we evaluate dust provenance through REE, Nd, Sr and Pb isotopes in three sections deposited during late Pleistocene-early Holocene across 700 km in the loess belt of the Pampean region in central Argentina. The isotopic comparison of loess from the three sections with southern South American (SSA) potential dust sources show that (1) sources from the southern Altiplano to latitudes of northern Patagonia supplied dust to the Pampas, (2) the slight Sr-Nd isotopic difference between fine and coarse loess may be attributable to grain size effects rather than to differences in provenance, and (3) higher mass accumulation rates in the Pampas are associated with an increased presence of dust originated in the southern Altiplano and southern Puna during the spans of 43-41 ka BP, 20-18 ka BP, 14.6-12.6 ka BP and 11.4-8.9 ka BP. We associate these rises in continental dust fluxes with climatic transitions from wetter to drier periods in the Puna-Altiplano Plateau related to synchronous climatic shifts to humid conditions at the Pampean Plain, probably triggered by El Niño-like conditions. The isotopic comparison with modern SSA dust indicates similar provenance compared to paleo-dust records, suggesting almost constant dust sources from MIS 3 to modern times and/or modest changes in the geochemical signature under the activation/deactivation of the different dust sources. Moreover, contrasting the isotopic signature of the loess sections with more distal palaeoarchives (i.e., South Atlantic Ocean marine sediment cores and Antarctic ice cores), the new data suggest that contrary to previous ideas, the Pampean Loess was not an important source of dust to these regions. Also, a common dust provenance during cold periods (e.g., Last Glacial Maximum and Antarctic Cold Reversal) supports the idea that changes in atmospheric transport efficiency can better explain dust flux variations observed over glacial/interglacial periods in distant palaeoarchives than changes in provenance.

Keywords

Radiogenic isotopes, unmixing model, South America, Pampean loess, provenance, dust, westerly, East Antarctica, Southern Ocean

1. Introduction

Atmospheric circulation is the major mechanism of heat transport on the Earth's surface, and tracing windblown dust from sources to depositional locations is the best means available for characterizing past wind circulation. Moreover, geological records of mineral dust enable the reconstruction of past dust fluxes and are therefore key to assessing its impact on the Earth system. The role of dust in forcing climate remains poorly understood and represents one of the largest uncertainties in climate model simulations (Heavens et al., 2012; Lee et al., 2016; Adebiyi and Kok, 2020). For the modeling and observational communities, paleo-dust records represent a large archive of information on the magnitude and spatial variability of dust deposition for the pre-observational era, as well as a way to validate dust models under different climate scenarios (e.g., Mahowald et al. 2006). Furthermore, clastic sediments have enormous potential to unravel past geological processes. Dust deposits provide valuable clues on paleoenvironmental settings such as continental aridity, glacial conditions, and dominant wind directions (e.g., An et al., 2001; Soreghan et al., 2002; 2008; 2014) and may provide analogues for desertification due to the ongoing global warming (e.g., D'Odorico et al., 2013). The provenance of wind-blown dust and its characteristics are key issues to understand climate, atmospheric and environmental changes (Lanci et al., 2020). Although sedimentary processes like weathering, erosion, transport, sedimentation and diagenesis are likely to modify to some extent the composition of sediments, it has been generally accepted that the chemical and isotopic compositions of sediments are still dominantly influenced by their source rocks (e.g., Ahmad et al., 2016). Accordingly, the chemical and isotopic compositions of paleo-dust records have been extensively used to decipher provenance (e.g., Bhatia, 1985; McLennan et al., 1993; Biscaye et al., 1997; Grousset et al., 1988, 1992, 1998; Grousset and Biscaye, 2005; Sun et al., 2005, 2010).

The southern portion of South America (SSA) features a number of environmental characteristics that allow the efficient production of fine particles: high relief, (semi)arid conditions with intermittent fluvial activity (Prospero et al., 2002; Ginoux et al., 2012; Gaiero, 2007; Cosentino et al., 2020; Lamy et al., 2019), and increased glacier activity during glacial

intervals (Ammann et al., 2001; Zech et al., 2017). The rain shadow effects caused by the last Andean uplift (i.e., since 26–28 Ma) created the 'South American arid diagonal' with average annual precipitation of roughly 250 mm (Blisniuk et al., 2005). This is a long and narrow region that extends from ~2º S in the Gulf of Guayaquil to ~53º S on the northern Tierra del Fuego island, following the coast in Ecuador to northern Chile, crossing into Argentina north and east of Santiago, and continuing southward through Patagonia. The major present-day dust source areas in SSA are located in a continuous N–S band of arid and semi-arid terrains coinciding with the arid diagonal (Prospero et al., 2002). Furthermore, SSA intersects two mayor zonal wind systems of the Southern Hemisphere: the Southern Westerly Winds (SWW) and the SubTropical Jet (STJ) (Fig. 1a). These expressions of the tropospheric circulation in the Southern Hemisphere are a key component of the global climate system, affecting precipitation, the Antarctic Circumpolar Current, and the global carbon cycle (e.g., Rojas, 2013; Toggweiler et al., 2006; Lamy et al., 2001; Menviel et al., 2018). In particular, the SWW play an important role in mid- and high-latitude atmosphere-ocean dynamics (Yuan et al., 2018), together with Southern Ocean buoyancy (Watson et al., 2015). These atmosphere-ocean processes control the upwelling of carbon-rich deep-water masses in the Southern Ocean, thereby affecting atmospheric CO_2 changes over glacial cycles (Anderson et al., 2009; Menviel et al., 2018) and the Holocene (Lamy et al. 2010; Saunders et. al. 2018).

Based exclusively on the Antarctic paleo-dust archive it is only possible to evaluate the spatial and temporal variability of mass deposition rates far from sources (e.g., Lambert et al., 2008). The attribution of this long-range paleo-dust to specific sources requires the chemical and/or physical characterization of potential source areas (PSAs) of dust during the past (e.g., Gaiero, 2007; Gili et al., 2017; Scheuvens et al., 2013; Chen et al., 2007; Aleinikoff et al., 2008). Reconstructions of dust provenance in ice cores from the Southern Hemisphere benefit from the geochemical differences between individual PSAs, revealing that SSA sources dominated the dust supply to the East Antarctic Plateau (Gaiero, 2007; Sudgen et al., 2009; Gili et al., 2016, 2017, 2022 under review; Koffmann et al., 2021; DeDeckker et al., 2021) and the South Atlantic Ocean (e.g., Noble et al., 2012; Anderson et al 2009; Peleari et al., 2019) during the last several glacial-

interglacial cycles. However, dust mass deposition rate variability in distal environments does not depend only on changes in dust provenance, but also on changes in the intensity of emissions from PSAs (Lambert et al., 2008; Delmonte et al., 2017) and in the intensity of the hydrologic cycle along atmospheric dust transport pathways (Markle et al., 2018). To disentangle the contributions of changes in dust provenance, dust emission intensity, and the hydrologic cycle intensity, it is necessary to complement the characterization of distal paleo-dust with that of close-to-source records.

In this contribution, our main objective is to constrain Late Quaternary SSA dust provenance to improve the interpretation of coeval dust records located in middle to distal environments, thus increasing knowledge on past atmospheric circulation over the Southern Hemisphere. To achieve this, we present for the first time a systematic analysis of rare earth elements (REE), strontium (Sr), neodymium (Nd) and lead (Pb) isotopes of Marine Isotope Stage 3 (MIS 3) to early Holocene loess samples from three sites that together describe proximal, intermediate and distal Pampean loess environments with respect to their PSAs. Furthermore, we revised the whole geochemical data set representing dust PSAs associated with the main winds affecting atmospheric circulation of SSA (i.e., SWW and STJ). We also considered other suggested sources (e.g., Zárate et al., 2003) associated with more restricted atmospheric circulation, as for example, the low-surface N-S circulation potentially deflating sediments from the Paraná River system, the Pampean Ranges, or the shores of Mar Chiquita Lake. Our new geochemical data and unmixing model reveal changes in the temporal and spatial distribution of fine dust deposited between MIS 3 and the early Holocene, refining the existing knowledge of dust sources and wind circulation changes in SSA.

2. Background: The origin of Pampean loess

Modern dust data single out the Pampean plains of SSA as a powerful dust sink (Cosentino et al., 2020). This has also been the case during the Quaternary, as evidenced by the extensive Pampean loess deposits across SSA (Zárate, 2003). Since the pioneering work of Teruggi (1957),

142 many researchers have been interested in understanding the Pampean loess origin (e.g., González-
143 Bonorino 1966; Iriondo, 1997; Krohling et al., 1999; Sayago et al., 2001; Zárate and Blasi, 1991,
144 1993; Zárate, 2003 and references therein). Based on mineralogical and/or stratigraphic features,
145 Patagonia, the Andean piedmont, the Pampean Ranges, Mar Chiquita Lake, and the Paraná River
146 Basin have been suggested as possible wind-borne sediment suppliers to the Pampean loess (e.g.,
147 González Bonorino 1965; Cantú and Degiovanni, 1984; Iriondo 1990; Cantú, 1992; Morrás 1997;
148 Krohling, 1999; Kirschbaum et al., 2000; Torre et al., 2020a). Apart from the source areas
149 previously mentioned, dust from the Altiplano region was also suggested to be entrained by slope
150 winds and carried aloft and eastward by the STJ, eventually being deposited across the eastern
151 plains (Bloom, 1990).

152 The first attempts to determine the provenance of the Pampean loess (~30-36º S, Fig. 1)
153 using geochemical data (e.g., REE and Sr-Nd isotopes) were made by Gallet et al. (1998) and
154 Smith et al. (2003). These works, however, lacked chronological control and hence, did not allow
155 for time-resolved provenance constraints. Also lacking a chronological framework, other studies
156 reported Sr-Nd isotopes (Delmonte et al., 2004) and Pb isotopic ratios (Gili et al., 2016) for
157 surface loess samples. Carter-Stiglitz et al. (2006) determined the first optically stimulated
158 luminescence (OSL) ages and Nd isotopes in loess-paleosols sequences located at lower latitudes
159 at the core of the Pampean loess (i.e., ~26ºS) (Fig. 1b), where the main atmospheric circulation
160 depends on the STJ (Smith et al., 2003). The first age model of Pampean loess was that of Torre
161 et al. (2019), which allowed time-resolved provenance determinations of the western Pampean
162 loess through REE (Torre et al., 2020a), and of an E-W Pampean loess transect based on grain
163 size characteristics (Torre et al., 2020b).

164 A primary conclusion from previous studies on the Pampean loess origin is that efforts
165 should be focused on the mineralogical/chemical/isotopic characterization of PSAs of SSA in
166 order to improve loess provenance studies. In this sense, Gili et al. (2016, 2017) have
167 characterized more than 50 samples from PSAs of SSA through Sr, Nd, Pb isotopes and REE with
168 the aim of constraining the provenance of paleo-dust records in the Southern Hemisphere. They
169 collected topsoil samples from desert terrains along a 4000-km-long latitudinal transect, which is

perpendicular to the main zonal atmospheric circulation (e.g., SWW and STJ) and includes the main sources of dust (i.e., Patagonia, the Andean piedmont in central-western Argentina and the Puna-Altiplano Plateau) to downwind settings such as the Pampas, the South Atlantic Ocean, the Southern Ocean and the East Antarctic Plateau. Moreover, geochemical data from other PSAs mentioned in the literature (e.g., Pampean Range rocks, Paraná suspended sediments, Mar Chiquita Lake sediments) are now included in the discussion about the origin of Pampean loess.

3. Sample locations and analytical procedures

3.1 Regional setting and loess sampling

The Pampean plains are located to the east of the Andes and are bounded to the west by the foothills of the Pampean Ranges and to the east by the South Atlantic Ocean (Fig. 1b). We based our sampling approach on previous age models (Kemp et al., 2004; 2006, Zárate et al., 2009) published for three loess sections across the Pampean loess belt, which we used to perform a 1-m vertical sampling centered at a depth corresponding to the previously reported Last Glacial Maximum (LGM, ~19-26 ka BP) for each site. Unfortunately, new ages have been determined for the new samples with significant differences compared to the previously published ones, and we now know that cover together a time spam from MIS 3 to the early Holocene, with only one site capturing the LGM (see the discussion in Torre et al., 2019).

Loess sampling for isotopes and REE was performed using thin-walled plastic cylindrical corers driven into the face of the sections at an average resolution of ~2.3 cm which is controlled by the external diameter of the plastic cylinders (see Supplementary Material, *S1*). The age of each sampled level for isotopes and REE determination was assigned through linear interpolation considering the mass accumulation rates for each dated interval (Torre et al., 2019). Numerical ages obtained by OSL methods are reported in Torre et al. (2019) (Supplementary Material, *S2*). The westernmost studied profile is Lozada (Lz, ~31°39′S; 64°08′W) (Fig. 1). This site is the closest to SSA's main dust sources to the west and is located in the foothills of the Pampean

198 Ranges, occupying a gentle slope (<3–5%) dissected by rivers and streams that drain the
199 mountains. From the total of 9.3-m of vertical outcrop, we sampled the section between 2.8 to 1.8
200 m below the surface. This loess section was deposited during the transition from the last
201 deglaciation to the early Holocene, between ~16.3 ka and 8.9 ka BP (Torre et al., 2019). The
202 Tortugas site is located 250 km SE of Lozada and represents the type section for the loess of the
203 central Pampas (Tr, ~32°43′S; 61°48′W) (Fig. 1). Here we sampled a 1-meter section between
204 2.2 and 1.2 m depth below the surface, deposited during the last deglaciation, between 19.5 ka
205 and 12.6 ka BP (Torre et al., 2019). The easternmost profile is exposed at the Gorina quarry (Gn,
206 ~34°54′S; 58°01′W) (Fig. 1), which has a more complex regional stratigraphic sequence (Tonni
207 et al., 1999) alternating between discrete loess and paleosol units (Zárate et al., 2002). The 1-
208 meter sampled section (e.g., between 1.6 and 0.6 m below the surface) was deposited during mid-
209 MIS 3 and the late LGM, between 47 ka and 22.1 ka BP (Torre et al., 2019).

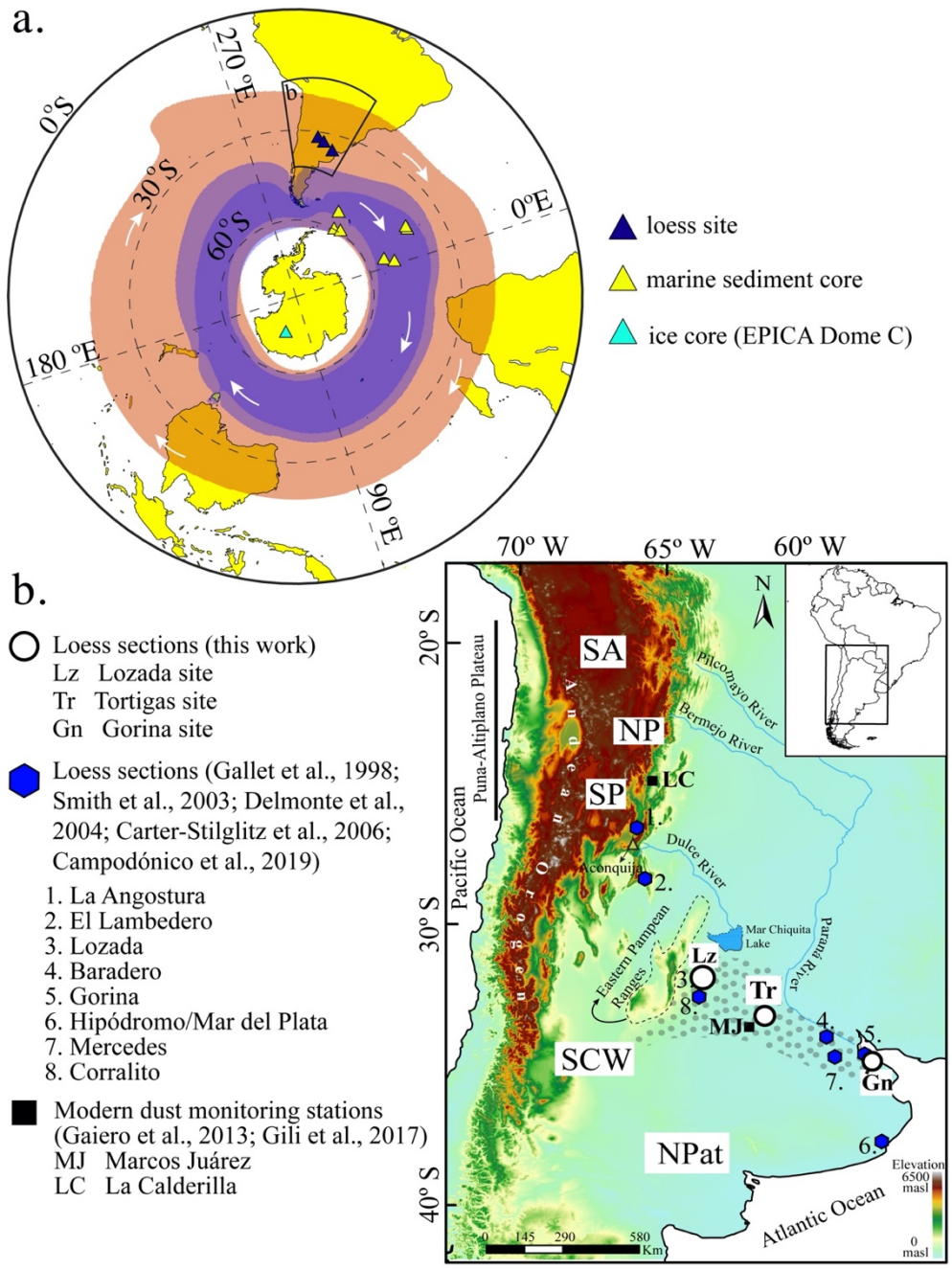

Figure 1. (a) Map showing the location of dust records and main wind belts from the Southern Hemisphere discussed in this paper. The lighter and darker blue-purple areas are delimited by the 7 ms^{-1} and 10 ms^{-1} contours of the E-W wind component at 850 hPa, respectively, and represent the South Westerly Winds. In turn, the reddish area is delimited by the 18 ms^{-1} contours of the E-W wind component at 200 hPa, and represents the SubTropical Jet. In all cases, contours represent the 1979-2020 climatological means calculated from monthly ERA5 reanalysis data. White arrows indicate general wind direction. (b) Map showing the location of the three loess sections studied in this work (white dots): Lz, Lozada; Tr, Tortugas and Gn, Gorina. The dotted area indicates the limits of the "loessic/loessoide" or "loess belt" sector of the Pampean region. The black squares are the present-day dust monitoring stations. Blue symbols indicate previously studied loess sites with available geochemical data.

211 *3.2 Grain size separation*

212

213 Highly time-resolved grain size analysis of loess samples reveals that loess deposited during
214 the late Pleistocene-early Holocene has multimodal distributions consistent with the existence of
215 multiple source areas and/or transport pathways (Torre et al., 2020b). When isotopic analyses are
216 made on bulk aeolian sediments (finer than 75 μm), the isotopic signature could be the result of
217 a mixture of sources with different grain sizes. To overcome this limitation, 10 loess samples
218 from Lozada and 10 from Tortugas were separated by a 44-μm sieve. The sieve diameter was
219 selected such that the fine and coarse grain size subpopulations were fully separated. Loess
220 samples from Gorina section were not split as they consist mainly of fine sediments (Torre et al.,
221 2020b).

222

223 *3.3 Isotopic analysis*

224

225 Sediments deposited in different environments are composed of mixtures of materials
226 (subpopulations) from different sources and/or transported by different mechanisms (Weltje,
227 1997 and references therein). In a previous work (Torre et al., 2020b), it was concluded that loess
228 samples from the Pampean region have multimodal grain size distributions consistent with the
229 existence of multiple source areas and/or atmospheric transport pathways. Following this idea, in
230 the present work we analyzed the isotopic composition of loess samples in two main grain size
231 subpopulations, in order to investigate possible isotopic changes according to changes in the
232 source areas and/or in the regional atmospheric circulation. For this purpose, fifty samples from
233 three loess records were analyzed for Nd and Sr isotopes and 18 for Pb isotopes. For Lozada and
234 Tortugas, isotopic analyses were performed for 10 fine (<44 um) and 10 coarse (>44 um) samples,
235 and 10 bulk samples were analyzed for Gorina. In order to better characterize the dust available
236 for long-range transport, Pb isotope ratios were analyzed on six and seven fine (<44 um) samples
237 from Lozada and Tortugas, respectively, and five bulk samples from Gorina.

Prior to samples digestion, an aqueous solution with ~3% H_2O_2 was used to eliminate organics, followed by 1 M HCl leach (overnight) to remove carbonates, then sampled were washed with Milli-Q water and dried. After this procedure, an aliquot of 100 mg of each sample was dissolved by tri-acid attack (HF-HNO_3-HCl) in Teflon Savillex® containers. Once in solution, Pb, Sr, and Nd were separated from the isotope aliquot using a sequence of ion chromatographic columns. We used Eichrom AG1-X8® 100-200 mesh anion exchange resin (for Pb), Eichrom TRU® resin (to separate REEs from major cations), Eichrom Sr® resin, and Eichrom LN® resin (for Nd).

Neodymium and Sr isotopic composition was determined by Thermal Ionization Mass Spectrometry (TRITON™ Plus) at the *Observatoire Midi-Pyrénées* (Toulouse, France). Isotope ratios were measured in dynamic mode, corrected for instrumental mass bias using $^{88}Sr/^{86}Sr$ = 0.1194 and $^{146}Nd/^{144}Nd$ = 0.7219. Chemical blanks for Sr and Nd isotopic measurements were below the detection limit. Pb isotope ratios were measured on a ThermoScientific NeptunePlus Inductively Coupled Plasma-Mass Spectrometer (ICP-MS) at Lamont-Doherty Earth Observatory (New York, USA). We used an Elemental Scientific APEX desolvator for Pb isotopic analyses. Measurements used Faraday static mode with 60 ratios per sample, with ~200 ppb Pb in 3% HNO_3 solutions, and ^{208}Pb beam were intensities between ~1.3 to 9 x 10-11 A. Pb samples were spiked with thallium (Tl) to achieve a Pb/Tl ratio of ~5.4. Tl isotopes were used to correct for mass fractionation using the exponential fractionation law and assuming $^{203}Tl/^{205}Tl$ = 0.41844 (Thirlwall 2002). Pb isotopes were measured at concentrations of 200 ng mL^{-1}, in 3% nitric acid solution.

All the isotopic data are corrected using the following values for international reference materials: NBS 987 for $^{87}Sr/^{86}Sr$; La Jolla for $^{143}Nd/^{144}Nd$ and BCR-2 for $^{206}Pb/^{204}Pb$, $^{207}Pb/^{204}Pb$, and $^{208}Pb/^{204}Pb$ ratios. These same reference materials bracketed each measured sample to assess instrumental drift and fractionation, and to determine data reproducibility. They were measured several times per run, yielding the following 2σ external errors. For $^{87}Sr/^{86}Sr$, two runs gave external errors of ± 0.000009. For $^{143}Nd/^{144}Nd$, the reproducibility varied during two measurement intervals with external errors of ± 0.000017. For $^{206}Pb/^{204}Pb$, three runs gave external errors of

0.00017, 0.00019 and 0.00013; for $^{207}Pb/^{204}Pb$, 0.00017, 0.00020 and 0.00014; for $^{208}Pb/^{204}Pb$, 0.00044, 0.00048 and 0.00040; for $^{207}Pb/^{206}Pb$, 0.000008, 0.000007; and for $^{208}Pb/^{207}Pb$, 0.000003 and 0.000004. Our measured NBS 987 $^{87}Sr/^{86}Sr$ is 0.710213 ± 0.000009 (n=3, 2σ). We also measured the La Jolla Nd standard twice, which gave $^{143}Nd/^{144}Nd = 0.511869 \pm 0.000017$. These values are within the 2σ error envelopes of the preferred values for these standards. Our measured BCR-2 Pb isotope values of $^{206}Pb/^{204}Pb = 18.7555 \pm 0.0001$, $^{207}Pb/^{204}Pb = 15.6216 \pm 0.0001$, and $^{208}Pb/^{204}Pb = 38.7107 \pm 0.0127$ (n = 6, 2σ), are within the 2σ error envelopes of unleached BCR-2 values: $^{206}Pb/^{204}Pb = 18.7529 \pm 0.0195$, $^{207}Pb/^{204}Pb = 15.6249 \pm 0.0040$, and $^{208}Pb/^{204}Pb = 38.7237 \pm 0.0004$, thus giving us confidence in the accuracy of our measurements.

For convenience, Nd isotope data are also reported here in units of $\varepsilon Nd = [(^{143}Nd/^{144}Nd_{measured} / {}^{143}Nd/^{144}Nd_{CHUR}) - 1] * 10^4$, where in this work we use $^{143}Nd/^{144}Nd_{CHUR} = 0.512638$ (Jacobsen and Wasserburg, 1980), rather than updated values (Bouvier et al., 2008) in order to be consistent with decades of published Nd isotope data. Also, for the three loess sites, grain size distributions were obtained for bulk samples (Torre et al., 2020b), which permits the calculation of a bulk isotopic composition that allows comparison between the isotopic signature of the three loess sections. For Tortugas and Lozada we averaged the isotope ratios of each grain size fraction for every analyzed sample, where fine and coarse isotopic ratios were previously multiplied by the relative abundance of each fraction.

3.4 Major and trace elements

Bulk loess samples from the Pampean Plain are finer than 75 μm (Torre et al., 2020b). A total of 61 bulk samples from the three studied loess sections were analyzed for REE. Determinations of REE for 22 samples from the Lozada section are reported in Torre et al. (2020a), while determinations for the samples of the other two sections (i.e., Tortugas and Gorina) are first reported in this study. Approximately 100 mg of each sample was introduced in carbon crucibles and were exposed to sodium peroxide (Na_2O_2) attack for 0.5 h in an oven at 490°C (Meisel et al., 2002). Once the fusion of the samples was achieved, they were taken into solution

294 by means of the addition of ultrapure HNO_3. The concentrations of REE in were determined by
295 ICP-MS Agilent 7500cx at National University of Córdoba (Córdoba, Argentina). Repeated
296 analyses (n = 7) of the AGV-2 and GSP-2 (USGS) rock standards show significant accuracy of
297 values to be on the order of 3%. The Eu anomaly (Eu/Eu*) was calculated as follows:
298 $Eu_N/(Sm_N \cdot Gd_N)^{0.5}$ (McLennan and Xiao, 1998), where the subindex N represents the element
299 normalized to the North American Shale Composite (NASC) (Wu et al., 2020). Sixteen loess
300 samples were dissolved by the alkaline fusion method ($Li_2B_4O_7$, 1050 °C, with HNO_3 dissolution)
301 and analyzed for major elements (i.e., P_2O_5 and TiO_2) by inductively coupled plasma with optical
302 emission spectroscopy (ICP-OES) at Lamont-Doherty Earth Observatory (New York, USA).
303
304 *3.5 Source end-member mixing calculation*
305
306 To quantify the contributions of dust from various sources, the isotope mixing model
307 SIMMR was used (Parnell, 2020). This model solves mixing equations for isotope data using a
308 Bayesian framework. Stable isotope mixing models have been widely used in zoology to provide
309 probabilistic estimates of source contributions to dietary mixtures (e.g., Kadye et al., 2020).
310 Recently, Pb isotope tracers gave satisfactory results using a Bayesian mixing model to analyze
311 dust provenance from the Pacific Ocean (Erhardt et al., 2020). This mixing model can be used to
312 determine the isotopic contribution of sources in a sediment mix and determine relative
313 contributions to the sediment provenance. For n isotopes, a unique solution can be calculated for
314 up to n+1 sources. The package SIMMR allows for the possible contribution of additional sources,
315 using an iterative approach to calculate all possible feasible solutions for any given sources and
316 isotopic mixtures, generating a distribution of feasible solutions (Inger et al., 2006). End members
317 were chosen as those regions likely contributing dust to the Pampean loess based on previous
318 isotopic studies (Gili et al., 2017; Gaiero et al., 2013).
319
320 **4. Results**
321

The REE concentrations of bulk (i.e., <75 μm) loess samples are listed in Table S1. Figure 2a-c shows REE loess composition normalized to the North American Shale Composite (NASC) (Wu et al., 2020). The loess samples from the three sections show similar flat REE NASC-normalized patterns, with positive Eu anomalies and negative Ce anomalies. The spider diagrams indicate that aeolian sediments from Tortugas (Fig. 2b) have homogeneous temporal REE compositions. On the other hand, loess samples from Lozada (Fig. 2a) and Gorina (Fig. 2c) show greater variability. The three sites show similar mean values for La/Yb: 0.83 for Lozada, 0.88 for Tortugas and 0.77 for Gorina, indicating slightly enrichments of heavy REEs compared to NASC. The UCC-normalized europium anomaly (Eu/Eu*) averages 1.13 ± 0.06, 1.20 ± 0.05 and 1.21 ± 0.13 for the <75 μm (bulk) fraction of Lozada, Tortugas and Gorina samples, respectively.

The radiogenic isotope data is shown in Table S2. The data indicates that Tortugas' $^{87}Sr/^{86}Sr$ is the highest in the fine (<44 μm) fraction ranging between 0.7080 and 0.7089, with an average value of ~0.7083 (Fig. 2d). For the same grain size fraction, the Lozada samples are slightly less radiogenic, ranging between 0.7078 and 0.7088 and with an average value of ~0.7081 (Fig. 2d). It is observed that for increasing loess particle size the $^{87}Sr/^{86}Sr$ is lower (Fig. 2e), this being more evident in particular for the Tortugas samples. The $^{87}Sr/^{86}Sr$ ratios for the Tortugas coarse fraction range between 0.7073 and 0.7076 with an average of ~0.7075, which is slightly lower than data from Lozada, which varies between 0.7077 and 0.7084, with an average ratio of 0.7081. The εNd values of the fine-grained Tortugas sediments range between -5.82 and -4.33, with an average of -5.08 ± 0.46, while the coarse-grained sediments range between -4.95 and -2.92 with an average of -3.99 ± 1.45 (Fig. 2e). Comparatively, εNd data for Lozada are slightly lower, showing fine loess ranging between -5.77 and -3.10 (average of -4.65 ± 1.73), while coarse sediments vary between -4.72 and -2.86 (average of -3.87 ± 1.45). For the three sections, the bulk isotopic composition of loess is quite similar, with $^{87}Sr/^{86}Sr$ (εNd) averages for Lozada, Tortugas and Gorina of 0.7081 (-4.36), 0.7079 (-4.58) and 0.7080 (-4.41), respectively (Fig. 2f).

The fine loess fractions from Lozada and Tortugas and bulk loess from Gorina display $^{208}Pb/^{207}Pb$ between 2.47-2.49 and $^{206}Pb/^{204}Pb$ between 1.195-1.205 (Fig. 2g-h). Unlike Sr and Nd,

Pb isotopes show a distinguishable signature among the loess samples from the three sites, showing a NW-SE trend of higher to lower values from Lozada to Gorina.

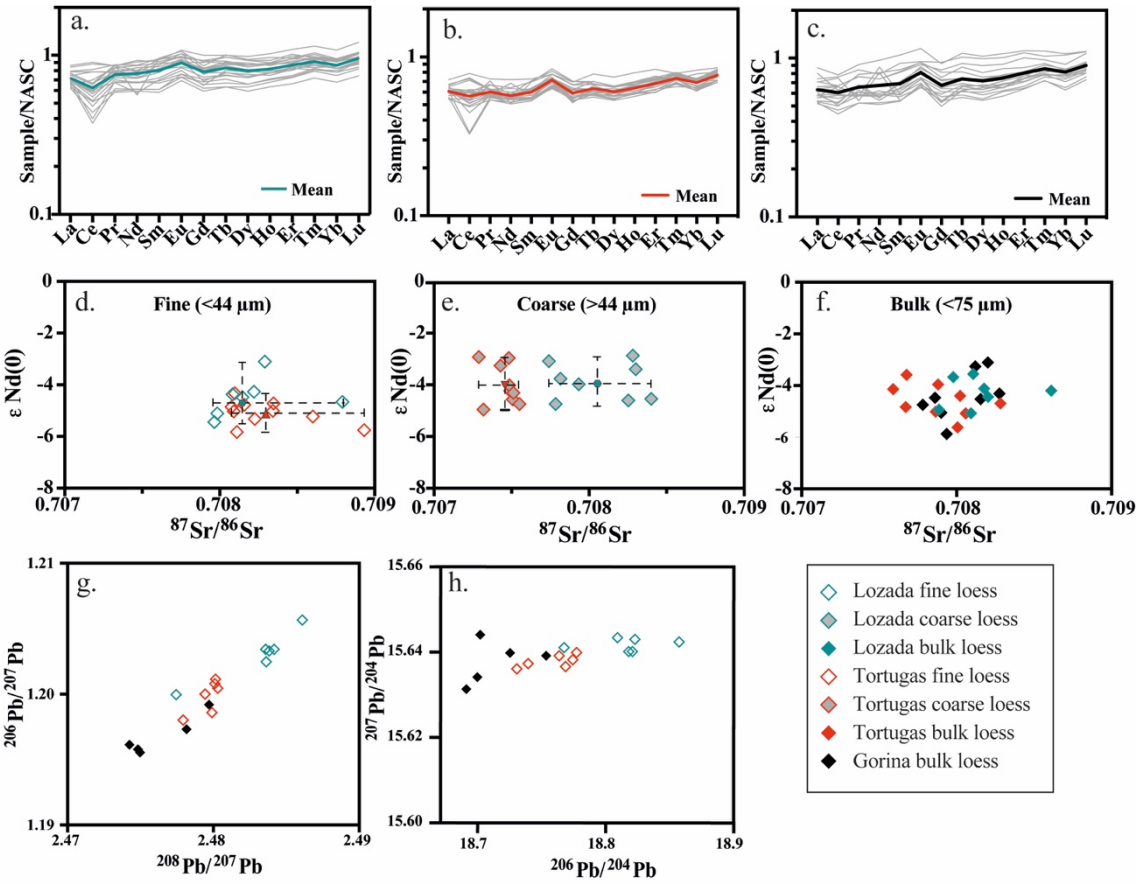

Figure 2. Rare Earth Element (REE) concentrations normalized to North American Shale Composite (NASC) (Wu et al., 2020) (a) Lozada, (b) Tortugas and (c) Gorina loess sections. $^{87}Sr/^{86}Sr$ and εNd results are shown for (d) fine fractions of Lozada and Tortugas sections, (e) coarse fractions of Lozada and Tortugas and (f) bulk fractiosn of Lozada, Tortugas and Gorina loess sections. Lead isotope ratios for fine fractions (<44 µm) of Lozada and Tortugas sections, and bulk (<75 µm) sediments from the Gorina profile (g-h).

5. Discussion

5.1. Rare earth elements as provenance tools

Rare earth elements have been widely used in provenance studies of atmospheric dust (e.g., Gallet et al., 1996, 1998; Humphries et al., 2020; Jahn et al., 2001; Pease and Tchakeria, 2002; van der Does et al., 2018; Zdanowicz et al., 2006; Campodonico et al., 2019). The importance of

359 this group of elements for sediment provenance studies lies in the fact that they are relatively
360 immobile during physical and chemical processes, serving as important markers in tracing
361 material sources and for characterizing the geochemical evolution of various systems (Khan et
362 al., 2017; Gwenzi et al., 2018). For distinguishing different aeolian dust sources, REE ratios are
363 more diagnostic than individual concentrations, as the former do not depend on dilution effects
364 of certain minerals (Ferrat et al., 2011).

365 Although the compositional field of most dust PSAs show good differentiation between
366 them, there is considerable overlapping between potential sources in the Paraná River basin,
367 southern central-western Argentina (S-CWA) and the Puna Plateau, thus precluding a distinctive
368 interpretation for the Pampean loess provenances (Fig. 3). The whole REE data set indicate
369 similar geochemical composition for the three loess sections (Fig. 2a-c, Fig. 3), and in agreement
370 with published data (i.e., Gallet et al., 1998; Smith et al., 2003; Campodónico et la., 2019),
371 pointing out that multiple sources could have supplied dust to the Pampean region between 47 ka
372 to 9 ka BP. Contrasting the geochemical composition of Lozada and the nearby Corralito section
373 (Campodónico et a., 2019) with those more local PSAs (e.g., shore sediments from Mar Chiquita
374 Lake, and riverine and lake sediments from the Pampean Ranges), Torre et al. (2020a) and
375 Campodónico et al. (2019) concluded that these sources were not significant dust contributors in
376 the past, pointing out that the Pampean loess of these localities derives mainly from Andean
377 sources. In the next section we further discuss loess provenance using isotopic data.

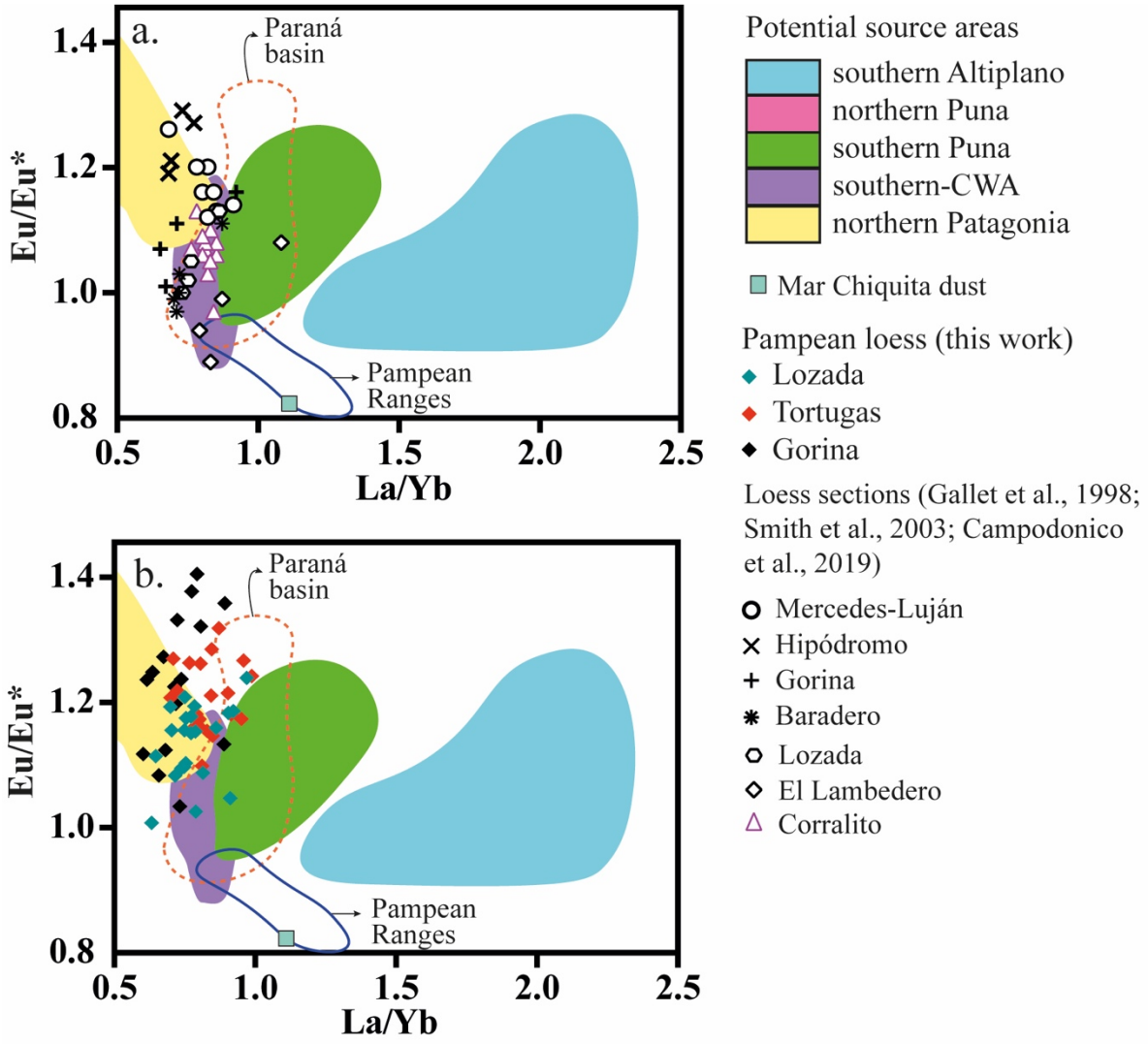

Figure 3. Rare earth element (REE) ratios characterizing dust sources from the Arid Diagonal (colored areas, Gili et al., 2017), the Paraná River basin (Campodonico et al., 2016; Depetris et al., 2003), Mar Chiquita Lake and eastern Pampean Ranges (Torre et al., 2020a). These data are compared with (a) previously published La/Yb vs Eu/Eu ratios of loess samples (Gallet et al., 1998; Smith et al., 2003; Campodónico et al., 2019) and (b) ratios from the Pampean loess for the Lozada, Tortugas and Gorina sites; white diamonds indicate average values for the three loess sections (Torre et al., 2020a and this work). All samples here are bulk fractions, represented by grain size fraction >75 μm.*

5.2 Sr and Nd isotopes applied to the provenance of the loess

Previous studies employed Sr and Nd isotopes to analyze the provenance of loess from different localities distributed in a wider region of the Pampas (Fig. 1b). Our new loess dataset allow for an update of previous observations made by Smith et al. (2003) and Gaiero (2007) indicating a general N-S trend for the mean εNd values recorded in loess samples from different latitudes (Fig. 4a). Compared with surface sediments from the PSAs, Nd isotopic data from

386 previous studies and this work show a clear N-S trend composition between a northern
387 Patagonia/S-CWA end-member and a Puna-Altiplano Plateau (PAP) end-member (Fig. 4a-b).
388 That is, the most southerly loess sites (i.e., Hipódromo and Mar del Plata), show a clear
389 Patagonian signal, while the most northernly loess sites (i.e., El Lambedero and La Angostura)
390 show a much more radiogenic $^{87}Sr/^{86}Sr$ and a less radiogenic εNd signature than samples located
391 to the south, both supporting a PAP origin. Interestingly, the loess Nd isotope ratios for samples
392 at intermediate latitudes (i.e., from 31°S to 36°S) do not strictly follow the N-S trend of a more
393 negative (positive) tendency towards the north (south), suggesting that multiple sources seem to
394 explain the loess provenance in the loess belt (Fig. 1b).

395 Combining our new data from all three sites and all grain size fractions, the average isotopic
396 values of 0.7080 ± 0.0114 for $^{87}Sr/^{86}Sr$ and -4.45 ± 0.84 for εNd are similar to values in loess
397 reported previously: 0.7084 ± 0.0008 for $^{87}Sr/^{86}Sr$, and -3.44 ± 1.11 for εNd (Smith et al., 2003);
398 and 0.7072 ± 0.0013 for $^{87}Sr/^{86}Sr$ and -2.96 ± 1.98 for εNd in bulk sediments (Gallet et al., 1998).
399 For the case of the <5 μm samples, average values are higher at 0.7099 ± 0.0010 for $^{87}Sr/^{86}Sr$ and
400 -2.02 ± 1.11 for εNd (Delmonte et al., 2004) (Fig. 4b and c). Although no age control is reported
401 for most of the previously published isotopic data, these data are very useful for improving loess
402 provenance evaluations. Compared to the published data set, our new data have a small range of
403 Sr and εNd isotopic variability (Fig. 4 c-d). The visual analysis of the new data set indicates that
404 multiple sources from SSA have likely contributed to all studied loess sites. At a first glance, the
405 Sr and Nd isotopic data allow us to discard northern Puna and the Paraná basin as significant dust
406 sources for the period under study (Fig. 4b), unlike the REE. Although some rocks from the
407 Pampean Range (e.g., amphibolite) have isotopic compositions similar to northern Patagonian
408 sediments and loess, the average composition from these rocks and the scarce abundance of
409 amphibolites within the Pampean Ranges (e.g., Toselli et al., 1986), do not support a significant
410 role as dust source areas to the Pampean region. Moreover, the low-level atmospheric circulation
411 over this mountainous sector is associated to N-S wind systems, arguing against any efficient
412 mechanism of dust transport to the eastern loess sites (e.g., Tortugas and Gorina). A significant
413 number of the loess samples have intermediate isotopic compositions aligned to a compositional

trend defined by the S-CWA/northern Patagonia and southern Altiplano end members (Fig. 4d). Based on Nd isotopic ratios of loess, the role of southern Puna as a source of dust to the Pampas cannot be ruled out considering that many loess samples show similar εNd ranges (i.e., -4.9 to -2.8).

Notably, the fine fractions of loess from Lozada and Tortugas have similar isotopic compositions, suggesting a common origin (Fig. 4d). This figure also shows that the fine sediments from Tortugas and, to a lesser extent from Lozada, have less (more) radiogenic εNd ($^{87}Sr/^{86}Sr$) ratios than its coarser fractions. This isotopic difference could be linked to changes of provenance or may be due to a grain size effect. The latter is often observed in fine sediment fractions showing high $^{87}Sr/^{86}Sr$ ratios due to higher values in minerals that tend be enriched in fine fractions and weathering effects (Clauer, 1979; Blum et al., 2003). The observed differences in $^{87}Sr/^{86}Sr$ ratios between fine and coarse Tortugas and Lozada loess (i.e., average differences of 0.0002 and 0.00008 respectively) is smaller than the variation indicated as a consequence of the grain size effect for similar sediment fractions (i.e., difference of ~0.0005 between fractions coarser and finer than 50 μm) (Feng et al., 2009). Thus, changes in the isotopic ratios of Sr of loess samples could be associated with wind-sorting effects and/or chemical weathering.

Figure 4d shows that the Tortugas samples have greater $^{87}Sr/^{86}Sr$ offsets between loess fractions compared to the Lozada samples. Accordingly, Tortugas loess has greater relative abundance of the fine (<44 μm) fraction (i.e., average 77%), compared to the same grain size fraction observed in Lozada (i.e., average 56%) (Torre et al., 2020b). Therefore, the Sr isotopic data supports the existence of a grain size effect in the Sr isotopic signal of the loess. This is less apparent in Nd isotopic ratios, which are less affected by sorting effects (Goldstein et al. 1984; Yokoo et al., 2004; Yang et al., 2005). The mean εNd difference between coarse and fine fractions is less than 1.1ε unit, in agreement with the observed small differences of ~1–2ε units between clay and silt for grain size fractions in river sediments (e.g. Bayon et al., 2015). In conclusion, although the bimodal grain size distributions in loess samples have been previously suggested to be linked to multiple sources (Torre et al., 2019), the isotopic difference between the finer and

441 coarser fractions is not significant enough to be considered a consequence of variations in
442 provenance.

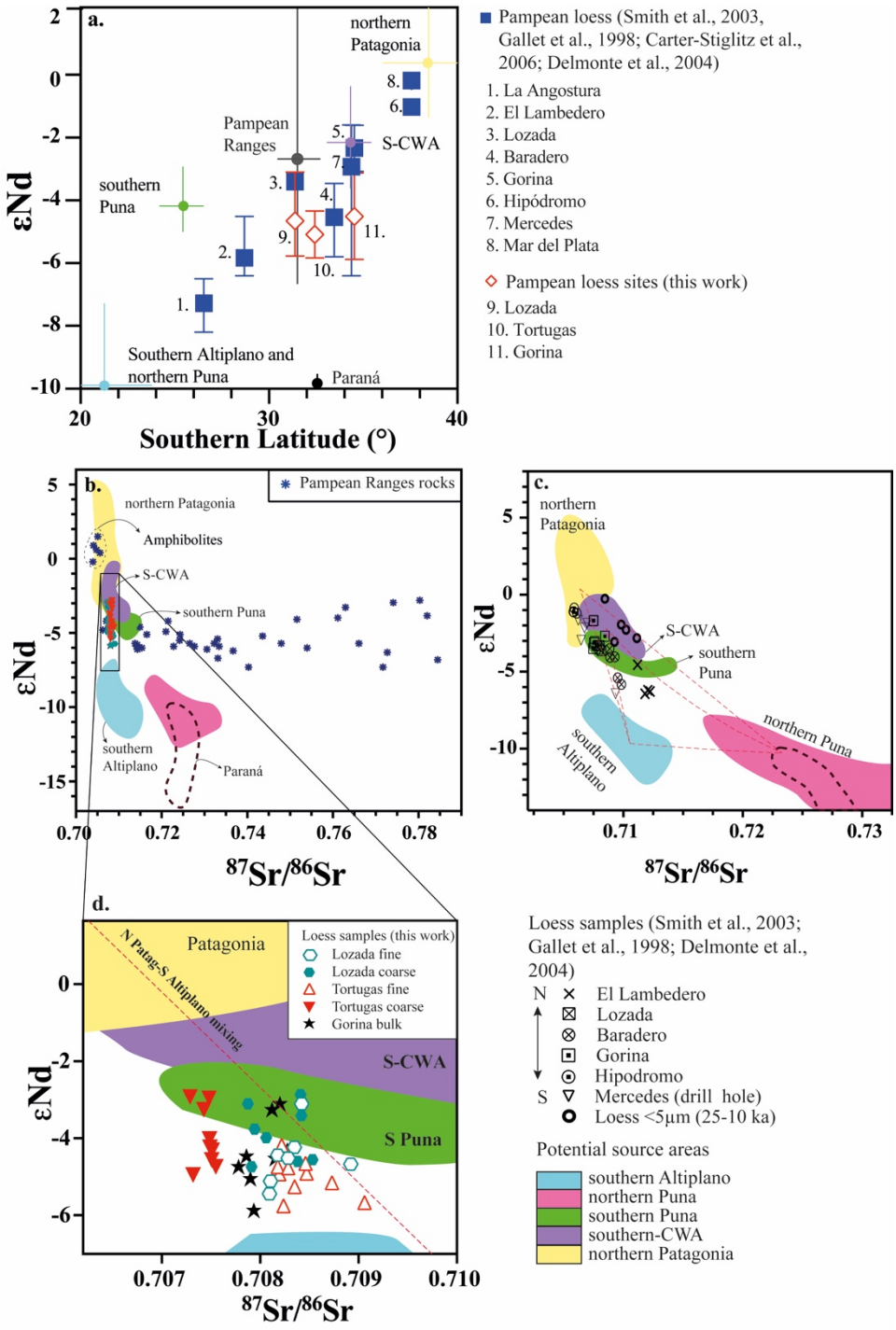

Figure 4. (a) Latitudinal εNd variation of Pampean loess. (b-d) Colored areas indicate the *isotopic fingerprint of southern South American dust sources from the arid diagonal (Gili et al., 2017), Paraná river sediments (Henry et al., 1996) and outcropping rocks from the Pampean Ranges (Rapela et al., 1998; Pankhurst et al., 1998; Grosse et al., 2002). These potential source areas are compared to: (c) previously published Sr and Nd isotope ratios of Pampean loess (Smith et al., 2003; Gallet et al., 1998; Delmonte et al., 2004), and (b and d) MIS 3-early Holocene Pampean fine (<44 µm) and coarse (>44 µm) loess from the Lozada and Tortugas sites, and bulk loess from the Gorina site (this work). Red-dashed lines are mixing lines between potential source areas calculated in Gili et al., (2017).*

443

444 *5.3. Pb isotope ratios applied to the provenance of loess*

445

446 In contrast to the Sr and Nd isotopic pair, the grain size dependence of Pb isotopes is not
447 well-documented, showing inconsistent results (e.g., Pettke et al., 2000; Unruh, 2001; Grousset
448 and Biscaye, 2005; Feng et al., 2010). Gili et al. (2016) showed that the differences between Pb
449 isotope ratios for the fine (<5 μm) and coarse (<63 μm) grain size fractions are small for most of
450 the PSAs from SSA and surface Pampean loess samples. The small differences observed between
451 the Pb isotopic compositions of the fine and coarse fractions of sediments from PSAs means that
452 sorting by size allows for attempts to relate the Pb isotope data in loess to the different PSAs. In
453 general, the Pb isotopic compositions of modern sediments in central and eastern SSA is
454 suspected to be anthropogenically contaminated by industrial emissions and leaded petrol
455 (Vallelonga et al., 2010). Thus, Pb isotopes in surface sediments from potential dust sources
456 representing Mar Chiquita Lake, and the Paraná basin and rivers draining the Pampean Ranges,
457 cannot be used for loess provenance analyses. These areas in any case have been found to be
458 insignificant sources of dust to the Pampean loess. Therefore, the following discussion involves
459 only Pb isotopic data of PSAs whose surface sediments are not suspected of anthropogenic
460 contamination.

461 Previously published Pb isotopes from loess samples showed compositions similar to S-
462 CWA and southern Puna, indicating a latitudinal trend from more to less radiogenic values
463 southward (Fig. 5a-b) (Gili et al., 2016). Data also indicate that fine-grained samples are less
464 radiogenic compared to the coarse fraction (<63μm) and bulk material (i.e., Gili et al., 2016;
465 Vallelonga et al., 2020), suggesting a grain size dependence on Pb isotopes.

466 Gili et al (2016), demonstrated that the differences between Pb isotope ratios for the fine and
467 coarse grain size fractions are small for most of the SSA samples. Based on this conclusion, we
468 focus the analysis of the Pb isotopic ratios in the fine loess fractions (i.e., <44 μm) (i.e., Lozada
469 and Tortugas), and the bulk fraction from the Gorina site. In term of $^{206}Pb/^{207}Pb$ and $^{206}Pb/^{204}Pb$,
470 Figure 5c-f shows the existence of a gradient from more radiogenic (Lozada) to less radiogenic
471 (Gorina) isotope ratios. Data from Tortugas show intermediate values, partially overlapping with

472 values from the two other sections. The whole dataset, including data from Gili et al. (2016) and
473 Vallelonga et al. (2010) (Fig. 5a-b, Fig. 5d-f), define a linear trend along the compositional fields
474 represented by S-CWA and southern Puna. The slope value of the linear array defined by loess
475 samples (i.e., 0.0406 ± 0.0140) is too low to signify an age (Pb isotope systematics require a slope
476 greater than 0.046). The fact that $^{207}Pb/^{204}Pb$ *vs* $^{206}Pb/^{204}Pb$ ratios from the Pampean sediments
477 cannot be interpreted as an isochron reinforces the idea of the supply of aeolian sediments from
478 more than one source area.

479 Figure 5 suggests that Pampean loess results from mixing of S-CWA and southern Puna.
480 This observation contrasts with the interpretation based on Sr and Nd isotopes, which indicate a
481 subordinate origin from the southern Altiplano (Fig. 4b-c). This inconsistency may be explained
482 by the spatial distribution of Pb isotopes, which might indicate that the sedimentary Pb isotopic

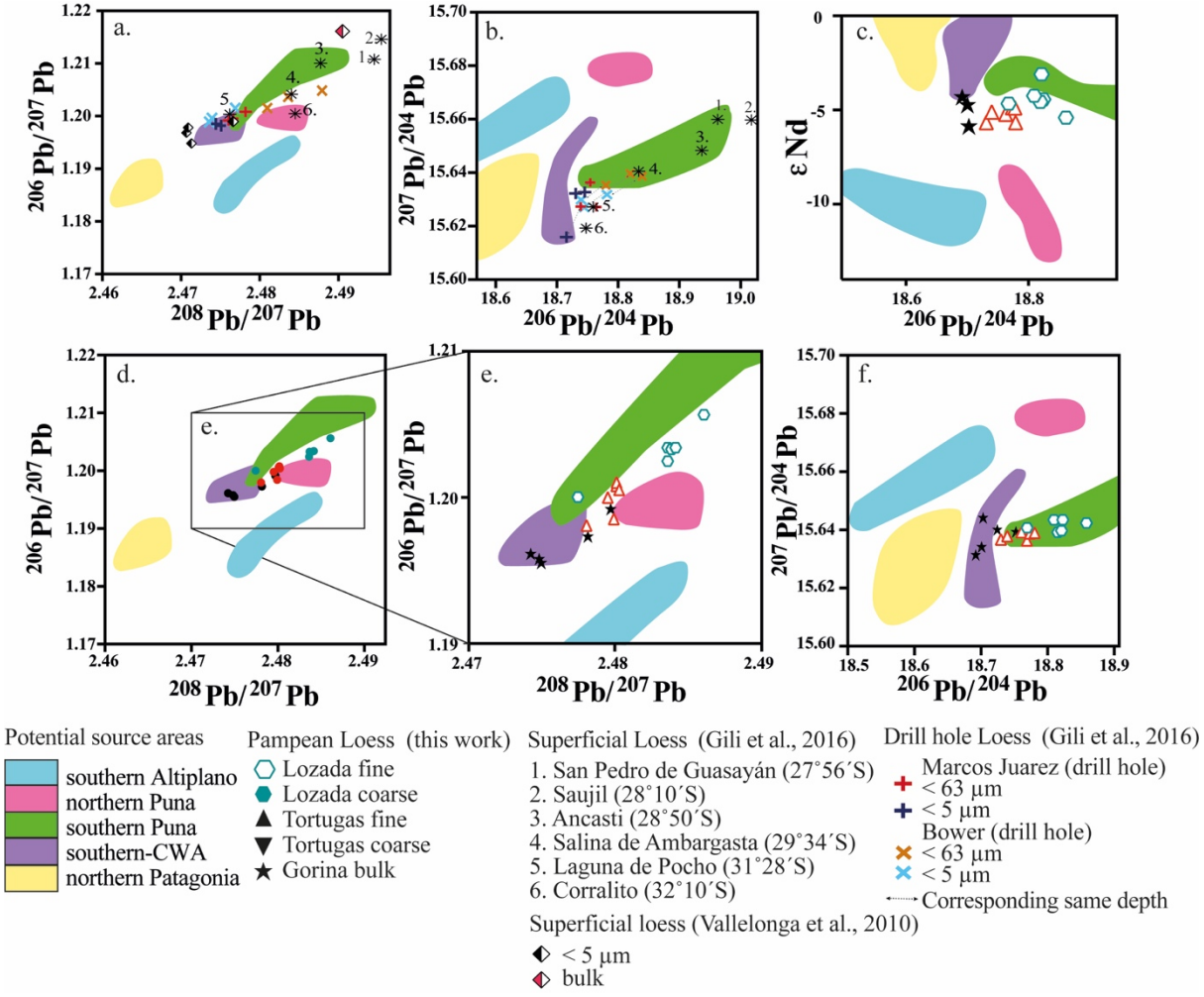

Figure 5. Lead isotope ratios for Pampean loess compared to potential dust source areas in southern South America (Gili et al., 2016).

budget is influenced by mineral sorting, thus obscuring dust provenance interpretations. In fact, the decreasing concentration of elements typically associated with heavy minerals such as zircons, monazites and allanites (i.e., P, La, Ce, Ti) with distance from the source (Fig. 6) supports the idea that the Pb isotopic signature is influenced by mineral sorting processes during aeolian transport. This is because heavy minerals tend to be enriched in the coarse sedimentary fraction (Garçon et al., 2014). While Gorina has systematically lower average concentrations compared to the Lozada data, similar concentrations of La and Ce are observed compared to the Tortugas loess record (Fig. 6). The similar concentrations between Tortugas and Gorina is also reflected in overlapping Pb isotope ratios between these two sites. Such a heavy mineral effect has already been noted for aeolian (Sun and Zhou, 2010; Bird et al., 2020) and fluvial transport processes (Garcon et al., 2013). In this sense, many coarse and dense minerals such as zircons, monazites, and allanites have more radiogenic Pb isotope ratios and are deposited closer to the source areas, whereas long-distance deposits are preferentially enriched in platy phyllosilicates and other slow-settling minerals. Thus, we suggest that the observed inverse correlation between Pampean loess Pb ratios and the distance to the sources might be caused in part by mineral sorting during aeolian transport. Future mineralogical studies in loess sites would help to assess the importance of Pb isotopes as a sediment provenance tool.

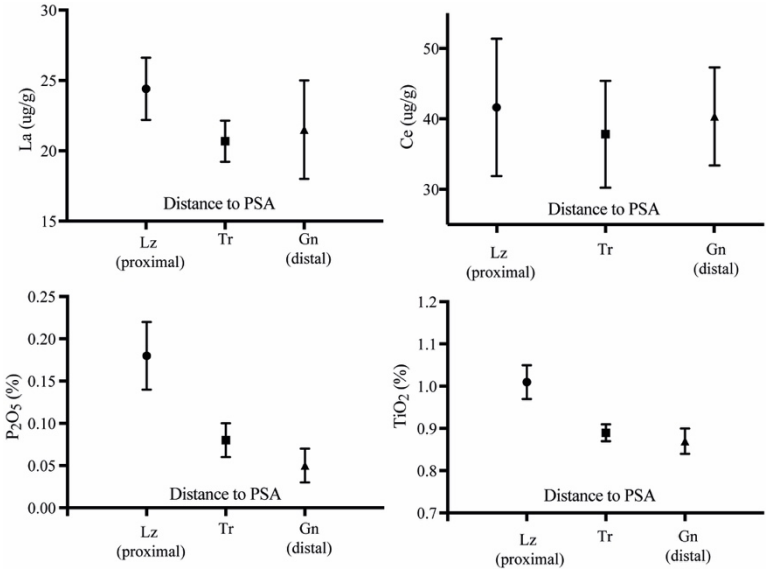

Figure 6. Average concentrations for each Pampean loess sampling site (Lz, n = 6; Tr and Gn, n = 5) of selected trace and major elements associated with heavy minerals. Error bars are 1σ based on the measured samples from each site.

5.4. Modern Pampean dust provenance for deciphering loess origin

Based on Sr-Nd isotopic fingerprinting, earlier studies showed that modern dust collected in the central Pampas (e.g., Marcos Juárez station, located 25 km W of the Tortugas site) (Fig. 1) is sourced from the southern Altiplano, and from S-CWA and/or southern Puna (Gaiero et al., 2013; Gili et al., 2017) (Fig. 7). These modern dust samples from the Marcos Juárez monitoring station (white diamonds in Fig. 7) have a 12-day mean sampling interval (Cosentino et al., 2020). Four of these samples have signatures consistent with a dust source from S-CWA while two other samples have clear southern Altiplano signatures. Interestingly, three samples indicate mixed signatures explained by S-CWA/southern Puna and southern Altiplano, similar to the isotopic compositions showed by loess samples from the three Pampean sections (grey area in Fig. 7). The average isotopic composition of modern dust (n = 12, black diamond, Fig. 7) has a similar εNd value to the Pampean loess, suggesting that similar sources (mainly S-CWA, southern Puna and southern Altiplano) were active from MIS3 to modern times. On the other hand, the $^{87}Sr/^{86}Sr$ ratio of the Pampean loess is lower than modern dust. The analyzed modern dust samples have almost half the grain size mode (Torre et al., 2020) compared to the fine fraction of loess, suggesting an important particle size control over the Sr isotope ratios of these samples.

The isotopic compositions of modern dust samples show that despite the short 12-day mean sampling period, these samples summarize the isotopic compositions of multiple PSAs, attesting to the extremely high temporal variability of dust sources deposited on the Pampean plain. Thus, the geochemical signature of each loess sample is an integration of the contribution of different dust sources (e.g., S-CWA, southern Puna and/or southern Altiplano) over time scales of hundreds to thousands of years. Based on the time resolution, each loess sample integrates time periods between 100-150 years at Lozada and Tortugas, and over ~600 years at Gorina (Torre et al., 2019).

After experimenting with the mixing of Sr-Nd composition of modern dust samples, we found that two extreme Marcos Juárez dust end members (e.g., two samples with clear northern Patagonia/S-CWA compositions and two samples with clear southern Altiplano compositions) permit us to obtain a mixing line that represents most of the compositions of the fine-grained Pampean loess (see calculation in Supplementary Material, *S3*) (Fig. 7). Moreover, a similar mixing experiment, combined with isotopic data from a dust sample collected in Buenos Aires province, supports the interpretation that northern Puna was insignificant as a dust source (Fig. 7). Furthermore, the isotopic mixing line based on the modern Marcos Juárez dust also helps to explain the composition of the coarse loess fraction. Notably, coarser sediments have an increased proportion of more radiogenic Nd sources (e.g., S-CWA and northern Patagonia), while the finer sediments are slightly closer to less radiogenic Nd sources (e.g., southern Altiplano). This mixing exercise ignores the role played by the southern Puna as a contributor of dust to the Pampas. This PSA has a clear N-S isotopic gradient (i.e., southernmost Puna has lower Nd and higher Sr isotope ratios than the northern sector of southern Puna as illustrated in Fig. 7) and hence, a possible contribution from the northern sector of southern Puna may be obscured as its composition lies within the mixing line closer to

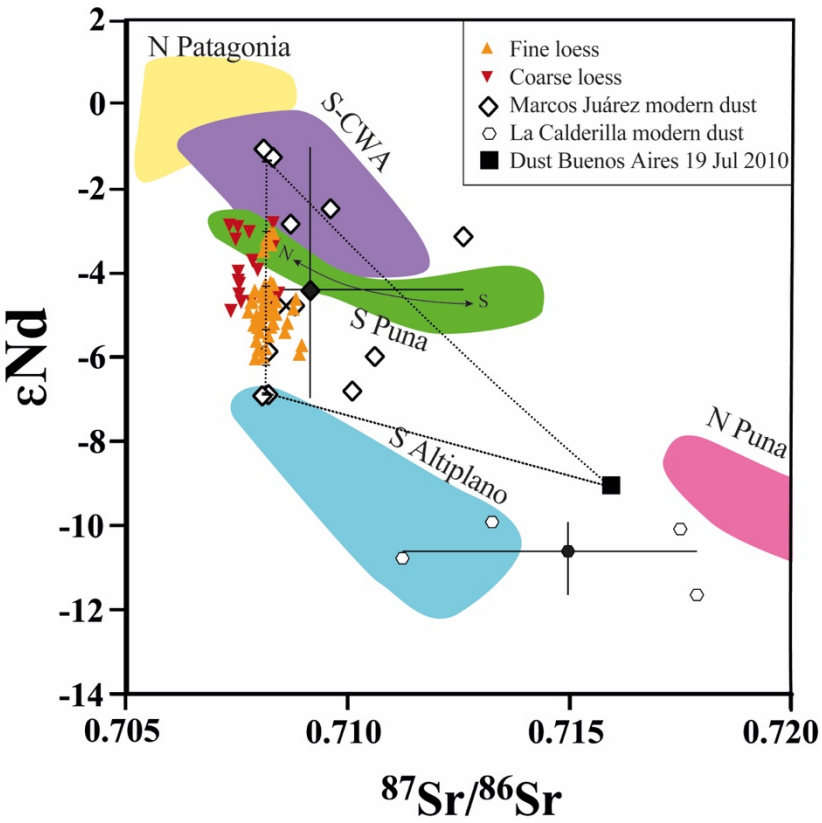

Figure 7. Nd-Sr isotope ratios of modern dust collected at the Marcos Juarez (diamonds) and La Calderilla (hexagons) monitoring stations (Gaiero et al., 2013; Gili et al., 2017). Black symbols represent the average composition and the range for each dust monitoring station. Dotted lines represent the calculated mixing curves between two end members from Marcos Juárez station, and between La Calderilla station. Data from La Calderilla representthe isotopic composition of dusts near their PAP source (Gili et al., 2017). Triangles indicate the Sr-Nd isotopic compositions of fine and coarse loess (this work).

560 the S-CWA/northern Patagonia end member.

561

562 *5.5. Short- and long-range deposition of southern South American dust*

563

564 Along with the Pampean loess, the isotopic compositions of MIS3-Holocene dust collected
565 in marine sediment cores from the Southern Atlantic Ocean and in ice cores of the eastern
566 Antarctic Plateau are consistent with the main provenance coming from SSA (Fig. 8) (Gili et al.,
567 2017, Noble et al., 2012; Walter et al., 2000; Delmonte et al., 2004, 2007, 2010). Among these
568 dust archives, the Pampean loess represents the proximal record of SSA dust (Li et al., 2008;
569 Albani et al., 2012), while South Atlantic Ocean and East Antarctic Plateau sedimentary deposits
570 respectively characterize the middle- and long-range dust transport from SSA. The restricted
571 isotopic variation shown by loess samples during MIS 3-early Holocene contrasts with the large
572 range of isotopic compositions of the medium-to-long range dust deposited during the same
573 period. Their increased range of Sr-Nd isotopes values are well-constrained by the isotopic
574 variability observed for the PSAs from SSA, indicating that these sources could have been
575 important dust suppliers. Furthermore, Sr-Nd isotopes indicate that there could have been sources
576 that supplied dust to more distal environments that are not recorded in the Pampean loess (e.g.,
577 northern Puna, southern Patagonia, Tierra del Fuego, southern Africa, New Zeland) (Sugden et
578 al., 2009; Noble et al., 2013; Koffman et al., 2021). The isotopic mismatch between Pampean
579 loess and the more distal archives may suggest that Pampean loess was not a significant dust
580 source to the distal environments during the past glacial-interglacial cycle as previously suggested
581 (Delmonte et al., 2010). This agrees with stratigraphic studies indicating no erosional hiatuses in
582 the Pampean loess record between MIS 3 and the early Holocene, meaning that deflation over the
583 Pampas was not widespread during this period (Torre et al. 2019, Zárate et al., 2009; Kemp et al.,
584 2004, 2006).

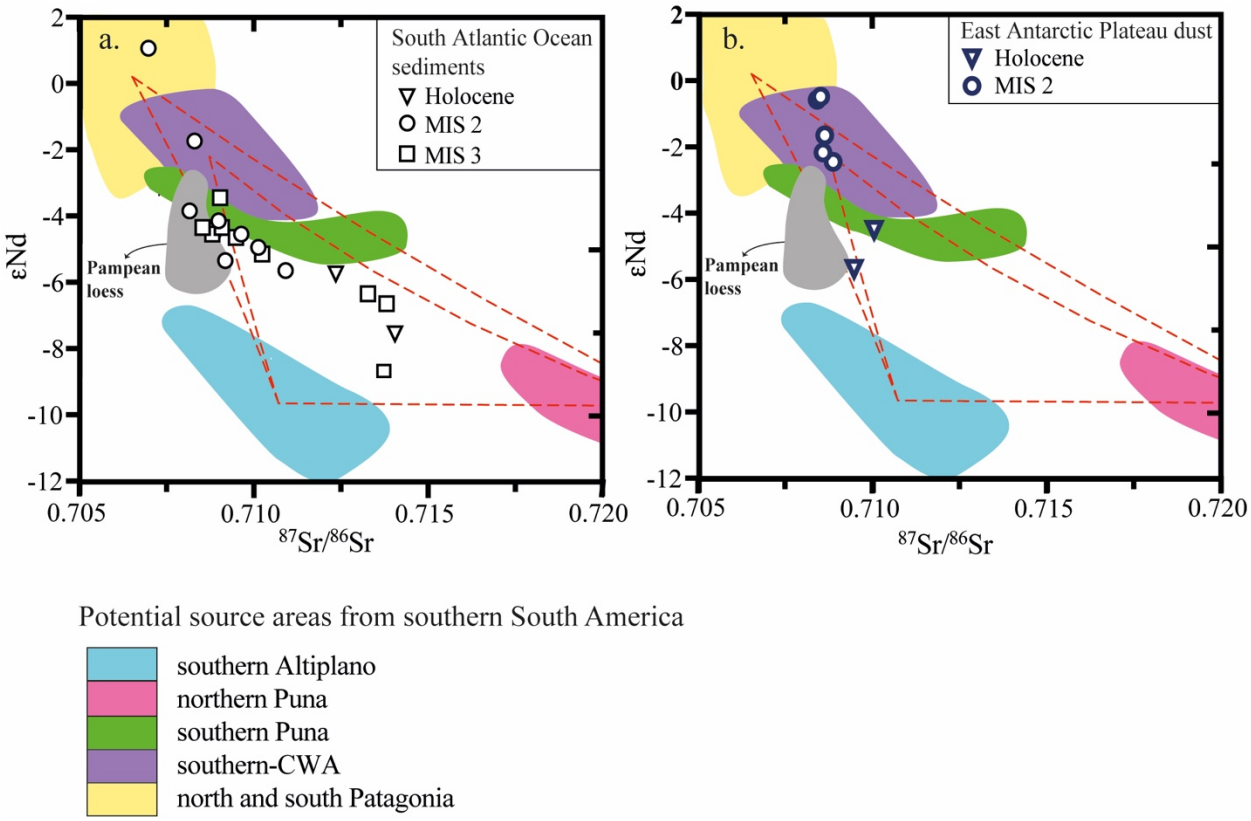

Figure 8. Sr-Nd isotopic signature of MIS 3 to Holocene Pampean loess deposits (grey area), together with (a) dust from marine sediment cores in the South Atlantic Ocean (Noble et al., 2012; Walter et al., 2000), and (b) dust from ice cores in the East Antarctic Plateau (Delmonte et al., 2004, 2007, 2008).

585

586 *5.6. Dust provenance unmixing*

587

588 Although the visual inspections of Figures 3-5 add critical observations to the understanding
589 of loess provenance, the quantitative apportionment of each source, as well as the potential to
590 identify the lesser prevalent dust sources, require additional techniques such as unmixing models.
591 We used the SIMMR unmixing model (Parnell et al., 2020) with PSAs of SSA. To constrain the
592 model we discarded, based on the discussions presented in sections *5.1* and *5.2*, the northern Puna,
593 Paraná River, Pampean Ranges and Mar Chiquita Lake PSAs, which were singled out as not
594 significant dust sources to the Pampean region.

595 As it was observed that there is a possible grain-size and mineralogical dependence of Sr and
596 Pb isotopic ratios in loess samples, here we contrasted SIMMR model results using only Nd
597 isotope data with results obtained combining Nd and Sr data. Interestingly, the results with and

without Sr isotope data were very similar. On the other hand, the model output obtained adding Pb isotopes is consistently different compared to the one using only Nd or the Nd-Sr isotopic pair. This is probably linked to the mineralogical sorting effect that we found in our data that could affect Pb isotopic system (section 5.3).

The statistical unmixing was performed on the fine loess samples from Lozada and Tortugas, and on bulk loess samples from the Gorina site. The unmixing model supports the existence of multiple dust sources to the Pampean loess (Fig. 9), indicating that none of the considered PSAs of SSA are negligible contributors of dust to the Pampas during MIS 3 to early Holocene (i.e., all of them show inputs greater than 10%) (Table S3) (see Supplementary Material, section *S4*). For the three loess sites, distal sources associated with the STJ circulation (i.e., southern Altiplano + southern Puna) represent the main dust suppliers (an average input of 55%) to Pampean loess deposited between MIS 3 and early Holocene. In turn, the model indicates that sources associated to the SWW circulation (i.e., S-CWA and northern Patagonia) have

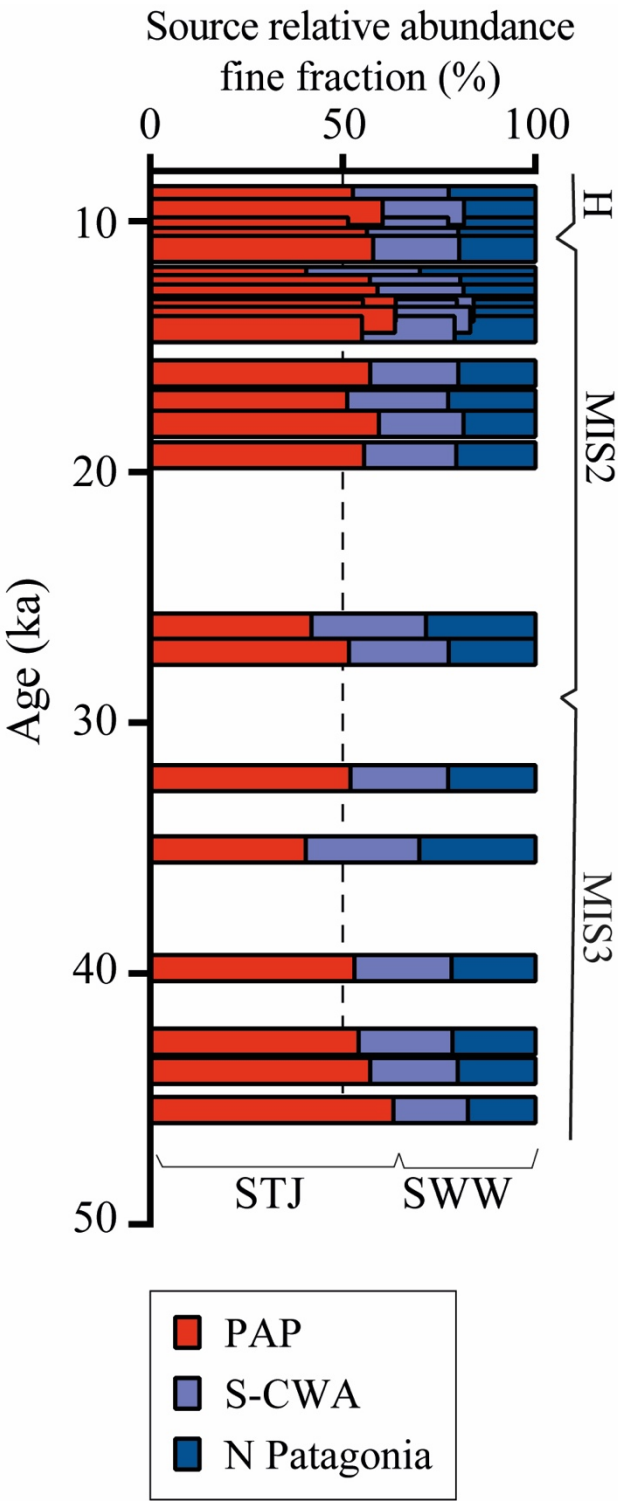

Figure 9. Analyses of the relative inputs of dust to the Pampean loess belt determined by the SIMMR unmixing model. The model was constrained with data of the fine fraction (<44 μm) from Lozada and Tortugas, and bulk loess from Gorina. The reddish colors indicate the proportion of dust supplied from sources interacting with the subtropical jet stream (STJ) (i.e., Puna-Altiplano Plateau, PAP). The purple colors indicate the proportion of dust supplied from sources interacting with the southern westerly winds (SWW) (i.e., southern central-west Argentina and northern Patagonia).

supplied an average of 45% of the dust reaching the studied Pampean sites.

5.7. Major dust fluxes to the Pampas under El Niño-like conditions

Figure 10 contrasts loess mass accumulation rates (MARs), loess provenance model outputs, lake levels reconstructions for Mar Chiquita Lake and lakes from the PAP area (e.g., proxies for humidity conditions over the Pampas and PAP respectively), and dust accumulation rates recorded at the South Atlantic Ocean and East Antarctic Plateau for the late Pleistocene to the early Holocene. Loess mass accumulation rates (MARs) varied substantially on millennial timescales (Fig. 10a) as a result of changes in dust availability at the sources, the intensity and/or position of the SWW or STJ, and/or dust settling/removing mechanisms (Torre et al., 2019). The three loess sections indicate that periods with increased MARs of the fine-grained fraction of dust are generally associated to increased dust contributions from PAP (e.g., up to ~64%) (Fig. 10d). This feature is clearly observed along the loess records in four different time windows; i.e., 43-41 ka BP; 20-18 ka BP (late MIS 2); 14.6-12.6 ka BP (Antarctic Cold Reversal); and 11.4-8.9 ka BP (early Holocene) (Fig. 10, shaded areas). Interestingly, the periods showing high dust fluxes over the Pampas are preceded by high lake level phases in the Altiplano (Fig. 10e-f) (Baker et al., 2001; Sylvestre et al., 1999; Fornari et al., 2001; Fritz et al., 2004; Placzek et al., 2006). Moreover, there is a positive trend between the relative magnitudes of preceding high-lake level events with increased MARs in the Pampean loess. For example, the most prominent humid Tauca phase (Fig. 10e) preceded the highest dust input recorded at Tortugas, which was mainly derived from the PAP region (~64%, Fig. 10d). In turn, the less intense Coipasa humid phase preceded the PAP source input of 60% observed at Lozada. Through these observations, we propose that high MARs observed in the Pampas are associated to preceding humid phases in the PAP region. Humid phases over the region caused significant accumulation of sediments on the lake shores, thus inducing a greater dust activity during the subsequent arid climatic phase.

If we assume that similar sources supplied dust both proximal and distal environments, it is likely that the relatively wet conditions in the Pampas from 13.5 ka until 8.5 ka BP (González et

al., 1994; Prado and Alberdi, 1999; Piovano et al., 2009; Cuña-Rodriguez et al., 2020) (Fig. 10b) enhanced wet dust deposition over proximal sectors (e.g., Pampas), thus reducing SSA-derived dust fluxes to more distal environments (compare Fig. 10a with Fig. 10g-h). This is also supported by high MARs detected in the distal loess site (Gorina) before 40 ka BP, which appears to be associated to a wet period, as indicated by soil development in NW Argentina (Zech et al., 2009a,b).

Although the Pampean loess has a persistent isotopic fingerprint consistent with a mixed provenance, the variability of this signature allows us to determine fluctuations in the contribution of these sources. The activation of the Puna+southern Altiplano dust sources occurs at times of increased MARs on loess deposits, suggesting the existence of a mechanism of enhanced deflation over the sources and/or increased wet removal of atmospheric dust downwind in the Pampean lowlands. This is compatible with the dominance of El Niño-like conditions in South America during the last glacial-interglacial cycle. In this sense, negative present-day rainfall anomalies are observed over the PAP during El Niño events, which are consistent with a stronger-than-average STJ over the Altiplano that hampers the advection of moisture from the eastern lowlands (Garreaud and Aceituno, 2007), enhancing deflation over the PAP region (e.g., Gaiero et al., 2013). In contrast, upper-level circulation anomalies tend to occur during La Niña episodes (Garreaud and Aceituno, 2007), enhancing moisture transport towards the Altiplano and favoring wetter-than-average conditions and lower dust emissions. El Niño Southern Oscillation (ENSO)-related rainfall anomalies at a global scale show that El Niño episodes are typically associated with anomalously wet conditions in the central-eastern portion of SSA (Ropelewski and Halpert, 1987), which in turn could have promoted increased scavenging of PAP-derived atmospheric dust over the Pampas (Torre et al., 2019).

There is no scientific consensus about past variability of ENSO conditions during the late Pleistocene and early Holocene. Nevertheless, from 38.2 to 8.4 ka BP strong El Niño-like manifestations have been infered from studies of alluvial sequences in the coastal region of southern Peru (Keefer et al., 1998; 2003; Ortlieb et al., 2003). Other studies have concluded that these records probably reflect local short-lived rainfall events, rather than through El Niño

episodes (Vargas et al., 2006). Moreover, reconstructions of temperature variability in the Pacific Ocean have indicated reduced ENSO conditions during the LGM compared to the Holocene (Ford et al., 2015). At the same time, some model simulations indicate intensified ENSO variability for this glacial period (e.g., Timmerman et al., 2004; Otto-Blesiner et al., 2003). Nonetheless, at millennial timescales, results from geological records and models still suggest persistent ENSO variability throughout the entire last glacial-interglacial cycle, and weaker frequencies and amplitudes of major El Niño-like events may have characterized the latest Pleistocene and the early Holocene compared to the late Holocene (Rodbell et al., 1999; Moy et al., 2002; Tudhope et al., 2001, Clement et al., 1999). Future studies of younger loess deposits spreading towards the mid-late Holocene could help in the identification of the influence of the ENSO variability on aeolian deposits between Late Pleistocene and Holocene times.

5.8. Lower dust input to the Pampas under equatorward-shifted SWW during the LGM and ACR

Many uncertainties still exist about the paleoclimatic conditions prevailing over SSA's dust PSAs during the LGM. This period is barely observed in the Gorina profile, with only two isotopic data points available for dust provenance analysis. The LGM is of great interest for the understanding of paleo-atmospheric circulation and the interaction between dust and climate because of the sharp increase of dust fluxes recorded in the South Atlantic Ocean and East Antarctic Plateau (e.g., Lambert et al., 2012) (Fig. 10g-h). In spite of geomorphological evidence (Zárate and Tripaldi, 2012; Tripaldi et al., 2011) and Earth system simulations (e.g., Albani et al., 2012) that support an important role for the S-CWA as a dust supplier during the LGM to the South Atlantic Ocean and East Antarctic Plateau (Fig. 8) (Gili et al., 2017), a similar dust flux increase is not observed during the LGM as recorded at the Gorina site (Torre et al., 2019). However, the unmixing model demonstrates a clear provenance change at the beginning of MIS 2, indicating increased inputs from S-CWA+northern Patagonia, representing more than 60% of the dust input to the Gorina site (Fig. 10c). We hypothesize that the lower dust deposition rates recorded over the continent between 47-43 ka BP, 40-22 ka BP, 17-14 ka BP and 12.3-11.4 ka

709 BP reflect reduced close-to-source dust wet deposition due to drier conditions at the Pampas
710 (Prieto, 2000; Behling, 2002; Iriarte, 2006; Behling and Pillar, 2007; Cuña-Rodriguez et al.,
711 2020). In turn, higher dust deposition rates at distal environments were probably facilitated by a
712 reduced hemispheric hydrological cycle that permitted longer lifetimes of atmospheric dust
713 particles (e.g., Lambert et al., 2008; Markle et al., 2018).

714 Reduced dust deposition at the Pampas with increased relative input from S-CWA+northern
715 Patagonia (i.e., ~62%) is also observed during a short time-lapse at the end of the ACR (Figs.
716 10a,d) . The activation of S-CWA+northern Patagonia sources during colder periods (i.e., LGM
717 and the ACR) was probably powered by an overall strengthening of Zonda winds induced by
718 more vigorous SWW, while they were shifted northward, closer to the equator (e.g., Gili et al.,
719 2017). Future studies of Pampean loess at higher temporal resolution during the LGM will help
720 to better understand dust dynamics during this important period in Earth's history.

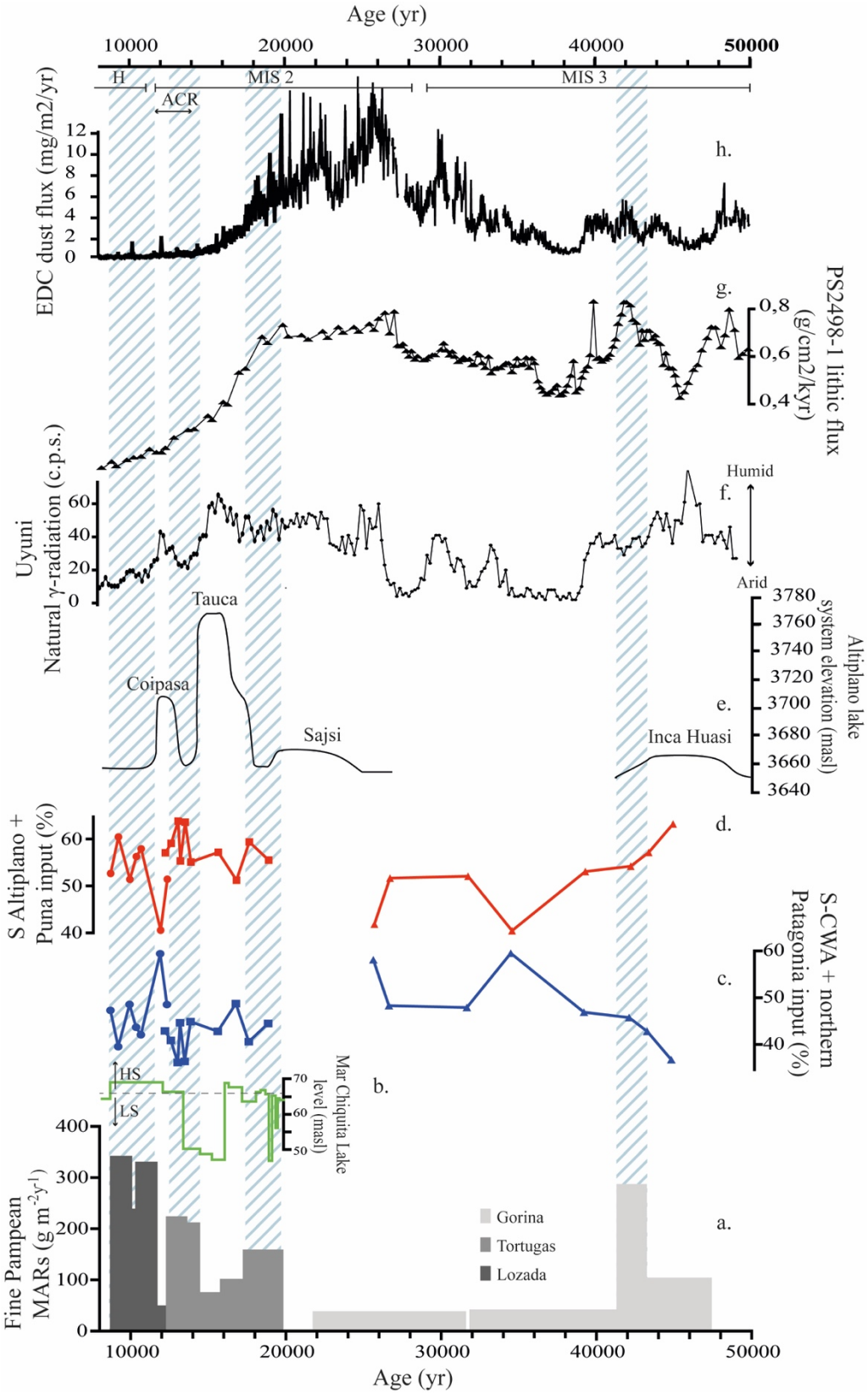

Figure 10. (a) Temporal variability of the mass accumulation rate (MAR) calculated for the fine dust fraction deposited on three Pampean loess sites. (b) Mar Chiquita Lake level (Cuña-Rodriguez et al., 2020). Contribution of dust derived from (c) south-central western Argentina (S-CWA) + northern Patagonia; and from (d) southern Altiplano + southern Puna the fine fraction of Pampean loess. (e,f) Paleo-lake levels in the Altiplano (Placzek et al., 2013; Baker et al., 2001). (g) Lithic fluxes at the South Atlantic Ocean (Anderson et al., 2014), and (h) dust fluxes at EPICA Dome C (EDC), East Antarctica (Lambert et al., 2012). Shaded areas denote times of high MAR.

721

5. Final remarks

The use of geochemical and unmixing model tools for understanding the provenance of the Pampean loess underlines the paleoclimatic importance of aeolian deposits for improving knowledge of past dust cycles. In SSA the loess belt is located at a relatively long distance from the Andean dust sources, and we have observed that mineral sorting effects on Pb isotopes obscures loess provenance interpretations. However, Pb isotopes combined with Sr-Nd isotopes allow us to deduce that multiple sources have supplied dust to the Pampean loess belt between MIS 3 and the early Holocene. Although REE are less diagnostic compared to radiogenic isotopes, they are complementary tools for loess provenance studies.

We observed that modern dust collected at the core of the Pampas has a similar geochemical composition to Pampean loess, suggesting that modern PSAs were also active during MIS 3 and the early Holocene, and that modest changes in the geochemical signature of loess respond to the activation/deactivation of the different dust sources. The data on modern dust and loess point to the northern Patagonia+S-CWA and southern Puna+southern Altiplano as the main dust suppliers to the Pampean loess. Our data excluded the northern Puna as an important Pampean loess dust supplier during the late Pleistocene. In order to improve the understanding on the behavior of the subtropical jet stream latitudinal movement, the absence of a northern Puna isotopic signature in loess samples along with the possible role play by the southern Puna should be further investigated.

The geochemical fingerprint of Pampean loess does not explain the entirety of the isotopic composition of dust in distal paleo-records located at the South Atlantic Ocean and the East Antarctic Plateau. This suggests that during the studied period the Pampean loess was not an important dust supplier to distal depositional environments and/or that there were active sources that not detected at the Pampean loess.

Revisiting geochemical data from previous loess studies along with new data from this study has permitted us to discard some PSAs located close to the Pampean loess (e.g., Mar Chiquita Lake, Paraná River, Pampean Range) as significant dust contributors to this region. Although the

Pampean loess record suggests that multiple SSA dust sources have been active during the past, the dominance of the S-CWA and the northern Patagonia signature on dust recovered from distal environments (e.g., Antarctica) point to the existence of a higher transport efficiency of the SWW during the last glacial period. During colder periods (e.g., the LGM and ACR), the activation of S-CWA/northern Patagonia sources could have been powered by the strengthening of the foehn Zonda wind, induced by a more vigorous SWW. We suggest that higher dust deposition rates at distal environments were promoted by a reduced hemispheric hydrological cycle that permitted longer airborne residence times of atmospheric dust particles and reduced close-to-source deposition.

Finally, the elevated dust deposition rates observed during some periods in the Pampas is interpreted as associated with the increased frequency/intensity of El Niño-like conditions. This allowed for sediment deflation from a dryer Puna-Altiplano region and deposition over the more humid Pampas.

Acknowledgments

This work was financially supported by SECyT-UNC, FONCyT (PICT 0525). It was also partly supported by the ECOS-MINCyT and CONICET-CNRS projects. G. Torre acknowledges support from Fulbright Program; and J. Prunier and A. Lojo for unconditional support in sample preparation and measurements. N. J. Cosentino acknowledges support from award ANID FONDECYT/POSTDOCTORADO 2020 #3200085. S. L. Goldstein acknowledges support from the Storke Endowment of the Department of Earth and Environmental Sciences, Columbia University.

References

Adebiyi, A. A., & Kok, J. F. (2020). Climate models miss most of the coarse dust in the atmosphere. *Science advances*, 6(15), eaaz9507. https://doi.org/10.1126/sciadv.aaz9507

Ahmad, I., Mondal, M. E. A., & Satyanarayanan, M. (2016). Geochemistry of Archean metasedimentary rocks of the Aravalli craton, NW India: Implications for provenance, paleoweathering and supercontinent reconstruction. *Journal of Asian Earth Sciences*, 126, 58-73. https://doi.org/10.1016/j.jseaes.2016.05.019

783 Albani, S., Mahowald, N.M., Delmonte, B. et al. Comparing modeled and observed
784 changes in mineral dust transport and deposition to Antarctica between the Last Glacial
785 Maximum and current climates. Clim Dyn 38, 1731–1755 (2012).
786 https://doi.org/10.1007/s00382-011-1139-5
787
788 Ammann, C., Jenny, B., Kammer, K., & Messerli, B. (2001). Late Quaternary glacier
789 response to humidity changes in the arid Andes of Chile (18–29 S). *Palaeogeography,*
790 *Palaeoclimatology, Palaeoecology*, 172(3-4), 313-326. https://doi.org/10.1016/S0031-
791 0182(01)00306-6
792
793 An, Z., Kukla, G., Porter, S.C. y Xiao, J. 1991. Late quaternary dust flow on the chinese
794 Loess Plateau. Catena 18: 125–132.
795
796 Anderson, R. F., Ali, S., Bradtmiller, L. I., Nielsen, S. H. H., Fleisher, M. Q., Anderson,
797 B. E., & Burckle, L. H. (2009). Wind-driven upwelling in the Southern Ocean and the
798 deglacial rise in atmospheric CO2. science, 323(5920), 1443-1448.
799 https://doi.org/10.1126/science.1167441
800
801 Anderson, R. F., Barker, S., Fleisher, M., Gersonde, R., Goldstein, S. L., Kuhn, G., ... &
802 Sachs, J. P. (2014). Biological response to millennial variability of dust and nutrient
803 supply in the Subantarctic South Atlantic Ocean. *Philosophical Transactions of the Royal*
804 *Society A: Mathematical, Physical and Engineering Sciences*, 372(2019), 20130054.
805 https://doi.org/10.1098/rsta.2013.0054
806
807 Armstrong-Altrin, J. S., Lee, Y. I., Verma, S. P., & Ramasamy, S. (2004). Geochemistry
808 of sandstones from the upper Miocene Kudankulam Formation, southern India:
809 Implications for provenance, weathering, and tectonic setting. *Journal of sedimentary*
810 *Research*, 74(2), 285-297. https://doi.org/10.1306/082803740285
811
812 Armstrong-Altrin, J. S., Machain-Castillo, M. L., Rosales-Hoz, L., Carranza-Edwards,
813 A., Sanchez-Cabeza, J. A., & Ruíz-Fernández, A. C. (2015). Provenance and depositional
814 history of continental slope sediments in the Southwestern Gulf of Mexico unraveled by
815 geochemical analysis. *Continental Shelf Research*, 95, 15-26.
816 https://doi.org/10.1016/j.csr.2015.01.003
817
818 Asiedu, D. K., Suzuki, S., & Shibata, T. (2000). Provenance of sandstones from the Lower
819 Cretaceous Sasayama Group, inner zone of southwest Japan. *Sedimentary*
820 *Geology*, 131(1-2), 9-24. https://doi.org/10.1016/S0037-0738(99)00122-0
821
822 Asiedu, D. K., Hegner, E., Rocholl, A., & Atta-Peters, D. (2005). Provenance of late
823 Ordovician to early Cretaceous sedimentary rocks from southern Ghana, as inferred from
824 Nd isotopes and trace elements. *Journal of African Earth Sciences*, 41(4), 316-328.
825 https://doi.org/10.1016/S0037-0738(99)00122-0
826
827 Baker, P., Rigsby, C., Seltzer, G. et al. Tropical climate changes at millennial and orbital
828 timescales on the Bolivian Altiplano. Nature 409, 698–701 (2001).
829 https://doi.org/10.1038/35055524
830
831 Bauluz, B., Mayayo, M. J., Fernandez-Nieto, C., & Lopez, J. M. G. (2000). Geochemistry
832 of Precambrian and Paleozoic siliciclastic rocks from the Iberian Range (NE Spain):

implications for source-area weathering, sorting, provenance, and tectonic setting. *Chemical Geology*, 168(1-2), 135-150. https://doi.org/10.1016/S0009-2541(00)00192-3

Bayon, G., Toucanne, S., Skonieczny, C., André, L., Bermell, S., Cheron, S., ... & Barrat, J. A. (2015). Rare earth elements and neodymium isotopes in world river sediments revisited. *Geochimica et Cosmochimica* Acta, 170, 17-38. https://doi.org/10.1016/j.gca.2015.08.001

Behling, H. (2002). South and southeast Brazilian grasslands during Late Quaternary times: a synthesis. *Palaeogeography, Palaeoclimatology, Palaeoecology*, 177(1-2), 19-27. https://doi.org/10.1016/S0031-0182(01)00349-2

Behling, H., & Pillar, V. D. (2007). Late Quaternary vegetation, biodiversity and fire dynamics on the southern Brazilian highland and their implication for conservation and management of modern Araucaria forest and grassland ecosystems. *Philosophical Transactions of the Royal Society B: Biological Sciences*, 362(1478), 243-251. https://doi.org/10.1098/rstb.2006.1984

Bhatia, M. R. (1985). Rare earth element geochemistry of Australian Paleozoic graywackes and mudrocks: provenance and tectonic control. *Sedimentary geology*, 45(1-2), 97-113. https://doi.org/10.1098/rstb.2006.1984

Biscaye, P. E., Grousset, F. E., Revel, M., Van der Gaast, S., Zielinski, G. A., Vaars, A., & Kukla, G. (1997). Asian provenance of glacial dust (stage 2) in the Greenland Ice Sheet Project 2 ice core, Summit, Greenland. *Journal of Geophysical Research: Oceans*, 102(C12), 26765-26781. https://doi.org/10.1029/97JC01249

Blum, J. D., & Erel, Y. (2003). Radiogenic isotopes in weathering and hydrology. *Treatise on geochemistry*, 5, 605. https://ui.adsabs.harvard.edu/link_gateway/2003TrGeo...5..365B/doi:10.1016/B0-08-043751-6/05082-9

Bouvier, A., Vervoort, J.D., Patchett, P.J., "The Lu–Hf and Sm–Nd isotopic composition of CHUR: Constraints from unequilibrated chondrites and implications for the bulk composition of terrestrial planets" EPSL 273 (2008) 48–57

Chen, J., Li, G., Yang, J., Rao, W., Lu, H., Balsam, W., ... & Ji, J. (2007). Nd and Sr isotopic characteristics of Chinese deserts: implications for the provenances of Asian dust. *Geochimica et Cosmochimica Acta*, 71(15), 3904-3914. https://doi.org/10.1016/j.gca.2007.04.033

Clauer, N. (1979). Relationship between the isotopic composition of strontium in newly formed continental clay minerals and their source material. *Chemical Geology*, 27(1-2), 115-124. https://doi.org/10.1016/0009-2541(79)90107-4

Clement, A. C., Seager, R., & Cane, M. A. (1999). Orbital controls on the El Nino/Southern Oscillation and the tropical climate. Paleoceanography, 14(4), 441-456.

Cosentino, N. J., Gaiero, D. M., Torre, G., Pasquini, A. I., Coppo, R., Arce, J. M., & Vélez, G. (2020). Atmospheric dust dynamics in southern South America: A 14-year modern dust record in the loessic Pampean region. *The Holocene*, 30(4), 575-588. https://doi.org/10.1177%2F0959683619875198

Cuña-Rodríguez, C., Piovano, E. L., García-Rodríguez, F., Sylvestre, F., Rostek, F., Bernasconi, S. M., & Ariztegui, D. (2020). Paleolimnological record of the Pampean plains (Argentina) as a natural archive of South American hydroclimatic variability since the LGM to the Current Warm Period. *Quaternary Science Reviews*, 250, 106675. https://doi.org/10.1016/j.quascirev.2020.106675

D'Odorico, P., Bhattachan, A., Davis, K. F., Ravi, S., & Runyan, C. W. (2013). Global desertification: drivers and feedbacks. *Advances in water resources*, 51, 326-344. https://doi.org/10.1016/j.advwatres.2012.01.013

Delmonte, B., Petit, J. R., Basile-Doelsch, I., Lipenkov, V., & Maggi, V. (2004). First characterization and dating of East Antarctic bedrock inclusions from subglacial Lake Vostok accreted ice. *Environmental chemistry*, 1(2), 90-94. https://doi.org/10.1071/EN04029

Delmonte, B., Petit, J. R., Basile-Doelsch, I., Jagoutz, E., & Maggi, V. (2007). 6. Late quaternary interglacials in East Antarctica from ice-core dust records. In *Developments in Quaternary Sciences* (Vol. 7, pp. 53-73). Elsevier. https://doi.org/10.1016/S1571-0866(07)80031-5

Delmonte, B., Andersson, P. S., Hansson, M., Schöberg, H., Petit, J. R., Basile-Doelsch, I., & Maggi, V. (2008). Aeolian dust in East Antarctica (EPICA-Dome C and Vostok): Provenance during glacial ages over the last 800 kyr. *Geophysical Research Letters*, 35(7). https://doi.org/10.1029/2008GL033382

Delmonte, B., Baroni, C., Andersson, P. S., Schoberg, H., Hansson, M., Aciego, S., ... & Frezzotti, M. (2010). Aeolian dust in the Talos Dome ice core (East Antarctica, Pacific/Ross Sea sector): Victoria Land versus remote sources over the last two climate cycles. *Journal of Quaternary Science*, 25(8), 1327-1337. https://doi.org/10.1002/jqs.1418

Delmonte, B., Paleari, C. I., Andò, S., Garzanti, E., Andersson, P. S., Petit, J. R., ... & Maggi, V. (2017). Causes of dust size variability in central East Antarctica (Dome B): Atmospheric transport from expanded South American sources during Marine Isotope Stage 2. *Quaternary Science Reviews*, 168, 55-68. https://doi.org/10.1016/j.quascirev.2017.05.009

Erhardt, A. M., Douglas, G., Jacobson, A. D., Wimpenny, J., Yin, Q. Z., & Paytan, A. (2021). Assessing sedimentary detrital Pb isotopes as a dust tracer in the Pacific Ocean. *Paleoceanography and Paleoclimatology*, 36(4), e2020PA004144. https://doi.org/10.1029/2020PA004144

Feng, J. L., Zhu, L. P., Zhen, X. L., & Hu, Z. G. (2009). Grain size effect on Sr and Nd isotopic compositions in eolian dust: implications for tracing dust provenance and Nd

model age. *Geochemical Journal*, 43(2), 123-131. https://doi.org/10.2343/geochemj.1.0007

Feng, J. L., Hu, Z. G., Cui, J. Y., & Zhu, L. P. (2010). Distributions of lead isotopes with grain size in aeolian deposits. *Terra Nova*, 22(4), 257-263. https://doi.org/10.1111/j.1365-3121.2010.00941.x

Ferrat, M., Weiss, D. J., Strekopytov, S., Dong, S., Chen, H., Najorka, J., ... & Sinha, R. (2011). Improved provenance tracing of Asian dust sources using rare earth elements and selected trace elements for palaeomonsoon studies on the eastern Tibetan Plateau. *Geochimica et Cosmochimica Acta*, 75(21), 6374-6399. https://doi.org/10.1016/j.gca.2011.08.025

Ford, H. L., Ravelo, A. C., & Polissar, P. J. (2015). Reduced El Niño–Southern oscillation during the last glacial maximum. *Science*, 347(6219), 255-258. https://doi.org/10.1126/science.1258437

Fornari, M., Risacher, F., & Féraud, G. (2001). Dating of paleolakes in the central Altiplano of Bolivia. *Palaeogeography, palaeoclimatology, palaeoecology*, 172(3-4), 269-282. https://doi.org/10.1016/S0031-0182(01)00301-7

Fritz, S. C., Baker, P. A., Lowenstein, T. K., Seltzer, G. O., Rigsby, C. A., Dwyer, G. S., ... & Luo, S. (2004). Hydrologic variation during the last 170,000 years in the southern hemisphere tropics of South America. *Quaternary Research*, 61(1), 95-104. https://doi.org/10.1016/j.yqres.2003.08.007

Gaiero, D. M., Probst, J. L., Depetris, P. J., Bidart, S. M., & Leleyter, L. (2003). Iron and other transition metals in Patagonian riverborne and windborne materials: geochemical control and transport to the southern South Atlantic Ocean. *Geochimica et Cosmochimica Acta*, 67(19), 3603-3623. https://doi.org/10.1016/S0016-7037(03)00211-4

Gaiero, D. M. (2007). Dust provenance in Antarctic ice during glacial periods: From where in southern South America?. *Geophysical Research Letters*, 34(17). https://doi.org/10.1029/2007GL030520

Gaiero, D. M., Brunet, F., Probst, J. L., & Depetris, P. J. (2007). A uniform isotopic and chemical signature of dust exported from Patagonia: Rock sources and occurrence in southern environments. *Chemical Geology*, 238(1-2), 107-120. https://doi.org/10.1016/j.chemgeo.2006.11.003

Gaiero, D. M., Simonella, L., Gassó, S., Gili, S., Stein, A. F., Sosa, P., ... & Marelli, H. (2013). Ground/satellite observations and atmospheric modeling of dust storms originating in the high Puna-Altiplano deserts (South America): Implications for the interpretation of paleo-climatic archives. *Journal of Geophysical Research: Atmospheres*, 118(9), 3817-3831. https://doi.org/10.1002/jgrd.50036

Gallet, S., Jahn, B. M., Lanoë, B. V. V., Dia, A., & Rossello, E. (1998). Loess geochemistry and its implications for particle origin and composition of the upper continental crust. *Earth and Planetary Science Letters*, 156(3-4), 157-172. https://doi.org/10.1016/S0012-821X(97)00218-5

Garcon, M., Chauvel, C., France-Lanord, C., Limonta, M., & Garzanti, E. (2013). Removing the "heavy mineral effect" to obtain a new Pb isotopic value for the upper crust. *Geochemistry, Geophysics, Geosystems*, 14(9), 3324-3333. https://doi.org/10.1002/ggge.20219

Garçon, M., Chauvel, C., France-Lanord, C., Limonta, M., & Garzanti, E. (2014). Which minerals control the Nd–Hf–Sr–Pb isotopic compositions of river sediments?. *Chemical Geology*, 364, 42-55. https://doi.org/10.1016/j.chemgeo.2013.11.018

Garreaud, R. D., & Aceituno, P. (2007). Atmospheric circulation over South America: mean features and variability. The physical geography of South America. *Oxford University Press*, Oxford, England.

Gili, S., Gaiero, D. M., Goldstein, S. L., Chemale Jr, F., Koester, E., Jweda, J., … & Kaplan, M. R. (2016). Provenance of dust to Antarctica: A lead isotopic perspective. *Geophysical Research Letters*, 43(5), 2291-2298. https://doi.org/10.1002/2016GL068244

Gili, S., Gaiero, D. M., Goldstein, S. L., Chemale Jr, F., Jweda, J., Kaplan, M. R., ... & Koester, E. (2017). Glacial/interglacial changes of Southern Hemisphere wind circulation from the geochemistry of South American dust. *Earth and Planetary Science Letters*, 469, 98-109. https://doi.org/10.1016/j.epsl.2017.04.007

Ginoux, P., Prospero, J. M., Gill, T. E., Hsu, N. C., & Zhao, M. (2012). Global-scale attribution of anthropogenic and natural dust sources and their emission rates based on MODIS Deep Blue aerosol products. *Reviews of Geophysics*, 50(3). https://doi.org/10.1029/2012RG000388

Gonzalez Bonorino, F. (1966). Soil clay mineralogy of the Pampa plains, Argentina. *Journal of sedimentary research*, 36(4), 1026-1035. https://doi.org/10.1306/74D715EB-2B21-11D7-8648000102C1865D

González MA (1994) Salinas del Bebedero basin (República Argentina). In: Kelts K, Gierlowski- Kordesch E (eds) Global Inventory of Lacustrine Basins. Cambridge University Press, Cambridge, UK.

Grousset, F. E., & Biscaye, P. E. (2005). Tracing dust sources and transport patterns using Sr, Nd and Pb isotopes. *Chemical Geology*, 222(3-4), 149-167. https://doi.org/10.1016/j.chemgeo.2005.05.006

Grousset, F. E., Biscaye, P. E., Zindler, A., Prospero, J., & Chester, R. (1988). Neodymium isotopes as tracers in marine sediments and aerosols: North Atlantic. *Earth and Planetary Science Letters*, 87(4), 367-378. https://doi.org/10.1016/0012-821X(88)90001-5

Grousset, F. E., Biscaye, P. E., Revel, M., Petit, J. R., Pye, K., Joussaume, S., & Jouzel, J. (1992). Antarctic (Dome C) ice-core dust at 18 ky BP: Isotopic constraints on origins. *Earth and Planetary Science Letters*, 111(1), 175-182. https://doi.org/10.1016/0012-821X(92)90177-W

Grousset, F. E., Parra, M., Bory, A., Martinez, P., Bertrand, P., Shimmield, G., & Ellam, R. M. (1998). Saharan wind regimes traced by the Sr–Nd isotopic composition of subtropical Atlantic sediments: last glacial maximum vs today. *Quaternary Science Reviews*, 17(4-5), 395-409. https://doi.org/10.1016/S0277-3791(97)00048-6

Gu, X. X. (1994). Geochemical characteristics of the Triassic Tethys-turbidites in northwestern Sichuan, China: implications for provenance and interpretation of the tectonic setting. *Geochimica et Cosmochimica Acta*, 58(21), 4615-4631. https://doi.org/10.1016/0016-7037(94)90195-3

Hao, Q., Guo, Z., Qiao, Y., Xu, B., & Oldfield, F. (2010). Geochemical evidence for the provenance of middle Pleistocene loess deposits in southern China. *Quaternary Science Reviews*, 29(23-24), 3317-3326. https://doi.org/10.1016/j.quascirev.2010.08.004

Heavens, N. G., Shields, C. A., & Mahowald, N. M. (2012). A paleogeographic approach to aerosol prescription in simulations of deep time climate. *Journal of Advances in Modeling Earth Systems*, 4(4). https://doi.org/10.1029/2012MS000166

Henry, F., Probst, J. L., Thouron, D., Depetris, P., & Garçon, V. (1996). Nd-Sr isotopic compositions of dissolved and particulate material transported by the Parana and Uruguay rivers during high (December 1993) and low (September 1994) water periods./Compositions isotopiques de Nd et Sr des matières en suspension et dissoutes transportées par les fleuves Parana et Uruguay en périodes de hautes (décembre 1993) et basses (septembre 1994) eaux. Sciences Géologiques, bulletins et mémoires, 49(1), 89-100.

Inger, R., Ruxton, G. D., Newton, J., Colhoun, K., Robinson, J. A., Jackson, A. L., & Bearhop, S. (2006). Temporal and intrapopulation variation in prey choice of wintering geese determined by stable isotope analysis. *Journal of Animal Ecology*, 75(5), 1190-1200. https://doi.org/10.1111/j.1365-2656.2006.01142.x

Iriarte, J. (2006). Vegetation and climate change Since 14,810 14C yr B.P. in southeastern uruguay and implications for the rise of early Formative societies. Quaternary Research, 65(1), 20-32. doi:10.1016/j.yqres.2005.05.005

Jacobsen, S. B., & Wasserburg, G. J. (1980). Sm-Nd isotopic evolution of chondrites. *Earth and Planetary Science Letters*, 50(1), 139-155. https://doi.org/10.1016/0012-821X(80)90125-9

Kadye, W. T., Redelinghuys, S., Parnell, A. C., & Booth, A. J. (2020). Exploring source differences on diet-tissue discrimination factors in the analysis of stable isotope mixing models. Scientific reports, 10(1), 1-17. https://doi.org/10.1038/s41598-020-73019-x

Keefer, D. K., DeFrance, S. D., Moseley, M. E., Richardson, J. B., Satterlee, D. R., & Day-Lewis, A. (1998). Early maritime economy and EL Niño events at Quebrada Tacahuay, Peru. S*cience*, 281(5384), 1833-1835. https://doi.org/10.1126/science.281.5384.1833

Keefer, D. K., Moseley, M. E., & DeFrance, S. D. (2003). A 38 000-year record of floods and debris flows in the Ilo region of southern Peru and its relation to El Niño events and great earthquakes. *Palaeogeography, Palaeoclimatology, Palaeoecology*, 194(1-3), 41-77. https://doi.org/10.1016/S0031-0182(03)00271-2

Kemp, R. A., King, M., Toms, P., Derbyshire, E., Sayago, J. M., & Collantes, M. M. (2004). Pedosedimentary development of part of a Late Quaternary loess-palaeosol sequence in northwest Argentina. *Journal of Quaternary Science: Published for the Quaternary Research Association*, 19(6), 567-576. https://doi.org/10.1002/jqs.848

Kemp, R., Zárate, M., Toms, P., King, M., Sanabria, J., & Arguello, G. (2006). Late Quaternary paleosols, stratigraphy and landscape evolution in the Northern Pampa, Argentina. Quaternary Research, 66(1), 119-132. doi:10.1016/j.yqres.2006.01.001

Lambert, F., Delmonte, B., Petit, J. et al. Dust-climate couplings over the past 800,000 years from the EPICA Dome C ice core. Nature 452, 616–619 (2008). https://doi.org/10.1038/nature06763

Lambert, F., Bigler, M., Steffensen, J. P., Hutterli, M., and Fischer, H.: Centennial mineral dust variability in high-resolution ice core data from Dome C, Antarctica, Clim. Past, 8, 609–623, https://doi.org/10.5194/cp-8-609-2012, 2012.

Lamy, F., Hebbeln, D., Röhl, U., & Wefer, G. (2001). Holocene rainfall variability in southern Chile: a marine record of latitudinal shifts of the Southern Westerlies. *Earth and Planetary Science Letters*, 185(3-4), 369-382. https://doi.org/10.1016/S0012-821X(00)00381-2

Lamy, F., Kilian, R., Arz, H. W., Francois, J. P., Kaiser, J., Prange, M., & Steinke, T. (2010). Holocene changes in the position and intensity of the southern westerly wind belt. *Nature Geoscience*, 3(10), 695-699. https://doi.org/10.1016/S0012-821X(00)00381-2

Lamy, F., Winckler, G., Alvarez Zarikian, C. A., & Scientists, E. (2019, December). Investigating the Dynamics of the Pacific Antarctic Circumpolar Current-Initial Results from International Ocean Discovery Program Expedition 383 (DYNAPACC). In *AGU Fall Meeting Abstracts* (Vol. 2019, pp. PP52A-07). https://doi.org/10.1016/S0012-821X(00)00381-2

Lanci, L., Delmonte, B., Salvatore, M. C., & Baroni, C. (2020). Insight Into Provenance and Variability of Atmospheric Dust in Antarctic Ice Cores During the Late Pleistocene From Magnetic Measurements. *Frontiers in Earth Science*, 8, 258. https://doi.org/10.3389/feart.2020.00258

Lee, P. K., & Yu, S. (2016). Lead isotopes combined with a sequential extraction procedure for source apportionment in the dry deposition of Asian dust and non-Asian dust. *Environmental Pollution*, 210, 65-75. https://doi.org/10.1016/j.envpol.2015.12.010

Li, F., Ginoux, P., & Ramaswamy, V. (2008). Distribution, transport, and deposition of mineral dust in the Southern Ocean and Antarctica: Contribution of major

sources. *Journal of Geophysical Research: Atmospheres*, 113(D10). https://doi.org/10.1029/2007JD009190

Li, G., Chen, J., Ji, J., Yang, J., & Conway, T. M. (2009). Natural and anthropogenic sources of East Asian dust. *Geology*, 37(8), 727-730. https://doi.org/10.1130/G30031A.1

Li, G., Pettke, T., & Chen, J. (2011). Increasing Nd isotopic ratio of Asian dust indicates progressive uplift of the north Tibetan Plateau since the middle Miocene. *Geology*, 39(3), 199-202. https://doi.org/10.1130/G31734.1

Mahowald, N. M., Muhs, D. R., Levis, S., Rasch, P. J., Yoshioka, M., Zender, C. S., & Luo, C. (2006). Change in atmospheric mineral aerosols in response to climate: Last glacial period, preindustrial, modern, and doubled carbon dioxide climates. *Journal of Geophysical Research: Atmospheres*, 111(D10). https://doi.org/10.1029/2005JD006653

Malusà, M. G., Resentini, A., & Garzanti, E. (2016). Hydraulic sorting and mineral fertility bias in detrital geochronology. Gondwana Research, 31, 1-19. https://doi.org/10.1016/j.gr.2015.09.002

Markle, B. R., Steig, E. J., Roe, G. H., Winckler, G., & McConnell, J. R. (2018). Concomitant variability in high-latitude aerosols, water isotopes and the hydrologic cycle. *Nature Geoscience*, *11*(11), 853-859. https://doi.org/10.1038/s41561-018-0210-9

McLennan, S. M., Hemming, S., McDaniel, D. K., & Hanson, G. N. (1993). Geochemical approaches to sedimentation, provenance, and tectonics. *Special Papers-Geological Society of America*, 21-21.

Menviel, L., Spence, P., Yu, J., Chamberlain, M. A., Matear, R. J., Meissner, K. J., & England, M. H. (2018). Southern Hemisphere westerlies as a driver of the early deglacial atmospheric CO 2 rise. *Nature Communications*, 9(1), 1-12. https://doi.org/10.1038/s41467-018-04876-4

Moy, C. M., Seltzer, G. O., Rodbell, D. T., & Anderson, D. M. (2002). Variability of El Niño/Southern Oscillation activity at millennial timescales during the Holocene epoch. *Nature*, 420(6912), 162-165. https://doi.org/10.1038/nature01194

Noble, A. E., Lamborg, C. H., Ohnemus, D. C., Lam, P. J., Goepfert, T. J., Measures, C. I., ... & Saito, M. A. (2012). Basin-scale inputs of cobalt, iron, and manganese from the Benguela-Angola front to the South Atlantic Ocean. *Limnology and oceanography*, 57(4), 989-1010. https://doi.org/10.4319/lo.2012.57.4.0989

Ortlieb, L., GuzmáN, N., & Marquardt, C. (2003). A longer-lasting and warmer interglacial episode during Isotopic Stage 11: marine terrace evidence in tropical western Americas. *Washington DC American Geophysical Union Geophysical Monograph Series*, 137, 157-180. https://ui.adsabs.harvard.edu/link_gateway/2003GMS...137..157O/doi:10.1029/137GM12

1177 Otto-Bliesner, B. L., Brady, E. C., Shin, S. I., Liu, Z., & Shields, C. (2003). Modeling El
1178 Niño and its tropical teleconnections during the last glacial-interglacial
1179 cycle. *Geophysical Research Letters*, 30(23). https://doi.org/10.1029/2003GL018553
1180
1181 Parnell, A. (2020). simmr: A Stable Isotope Mixing Model. R package version 0.4.5.
1182 https://cran.r-project.org/web/packages/simmr/index.html
1183
1184 Paleari, C. I., Delmonte, B., Andò, S., Garzanti, E., Petit, J. R., & Maggi, V. (2019).
1185 Aeolian dust provenance in central East Antarctica during the Holocene: Environmental
1186 constraints from single-grain Raman spectroscopy. *Geophysical Research*
1187 *Letters*, 46(16), 9968-9979. https://doi.org/10.1029/2019GL083402
1188
1189 Pettke, T., Halliday, A. N., Hall, C. M., & Rea, D. K. (2000). Dust production and
1190 deposition in Asia and the north Pacific Ocean over the past 12 Myr. *Earth and Planetary*
1191 *Science Letters*, 178(3-4), 397-413. https://doi.org/10.1016/S0012-821X(00)00083-2
1192
1193 Pin, C., Briot, D., Bassin, C., & Poitrasson, F. (1994). Concomitant separation of
1194 strontium and samarium-neodymium for isotopic analysis in silicate samples, based on
1195 specific extraction chromatography. *Analytica Chimica Acta*, 298(2), 209-217.
1196 https://doi.org/10.1016/0003-2670(94)00274-6
1197
1198 Piovano, E. L., Ariztegui, D., Córdoba, F., Cioccale, M., & Sylvestre, F. (2009).
1199 Hydrological variability in South America below the Tropic of Capricorn (Pampas and
1200 Patagonia, Argentina) during the last 13.0 ka. In Past climate variability in South America
1201 and surrounding regions (pp. 323-351). *Springer, Dordrecht*.
1202 https://doi.org/10.1007/978-90-481-2672-9_14
1203
1204 Placzek, C., Quade, J., & Patchett, P. J. (2006). Geochronology and stratigraphy of late
1205 Pleistocene lake cycles on the southern Bolivian Altiplano: implications for causes of
1206 tropical climate change. *Geological Society of America Bulletin*, 118(5-6), 515-532.
1207 https://doi.org/10.1130/B25770.1
1208
1209 Prado, J. L., & Alberdi, M. T. (1999). The mammalian record and climatic change over
1210 the last 30,000 years in the Pampean Region, Argentina. *Quaternary International*, 57,
1211 165-174. https://doi.org/10.1016/S1040-6182(98)00057-3
1212
1213 Prieto, A. R. (2000). Vegetational history of the Late glacial–Holocene transition in the
1214 grasslands of eastern Argentina. *Palaeogeography, Palaeoclimatology,*
1215 *Palaeoecology*, 157(3-4), 167-188. https://doi.org/10.1016/S0031-0182(99)00163-7
1216
1217 Prospero, J. M., Ginoux, P., Torres, O., Nicholson, S. E., & Gill, T. E. (2002).
1218 Environmental characterization of global sources of atmospheric soil dust identified with
1219 the Nimbus 7 Total Ozone Mapping Spectrometer (TOMS) absorbing aerosol
1220 product. *Reviews of geophysics*, 40(1), 2-1. https://doi.org/10.1016/S0031-
1221 0182(99)00163-7
1222
1223 Rodbell, D. T., Seltzer, G. O., Anderson, D. M., Abbott, M. B., Enfield, D. B., &
1224 Newman, J. H. (1999). An~ 15,000-year record of El Niño-driven alluviation in
1225 southwestern Ecuador. *Science*, 283(5401), 516-520.
1226 https://doi.org/10.1126/science.283.5401.516

Rojas, M. (2013). Sensitivity of Southern Hemisphere circulation to LGM and 4× CO2 climates. *Geophysical Research Letters*, 40(5), 965-970. https://doi.org/10.1002/grl.50195

Ropelewski, C. F., & Halpert, M. S. (1987). Global and regional scale precipitation patterns associated with the El Niño/Southern Oscillation. *Monthly weather review*, 115(8), 1606-1626. https://doi.org/10.1175/1520-0493(1987)115%3C1606:GARSPP%3E2.0.CO;2

Saunders, K. M., Roberts, S. J., Perren, B., Butz, C., Sime, L., Davies, S., ... & Hodgson, D. A. (2018). Holocene dynamics of the Southern Hemisphere westerly winds and possible links to CO 2 outgassing. *Nature Geoscience*, 11(9), 650-655. https://doi.org/10.1038/s41561-018-0186-5

Sayago, J. M., Collantes, M. M., Karlson, A., & Sanabria, J. (2001). Genesis and distribution of the Late Pleistocene and Holocene loess of Argentina: a regional approximation. *Quaternary International*, 76, 247-257. https://doi.org/10.1038/s41561-018-0186-5

Scheuvens, D., Schütz, L., Kandler, K., Ebert, M., & Weinbruch, S. (2013). Bulk composition of northern African dust and its source sediments—A compilation. *Earth-Science Reviews*, 116, 170-194. https://doi.org/10.1016/j.earscirev.2012.08.005

Smith, J., Vance, D., Kemp, R. A., Archer, C., Toms, P., King, M., & Zárate, M. (2003). Isotopic constraints on the source of Argentinian loess–with implications for atmospheric circulation and the provenance of Antarctic dust during recent glacial maxima. *Earth and Planetary Science Letters*, 212(1-2), 181-196. https://doi.org/10.1016/S0012-821X(03)00260-7

Soreghan, M. J., Soreghan, G. S., & Hamilton, M. A. (2002). Paleowinds inferred from detrital-zircon geochronology of upper Paleozoic loessite, western equatorial Pangea. *Geology*, 30(8), 695-698. https://doi.org/10.1130/0091-7613(2002)030%3C0695:PIFDZG%3E2.0.CO;2

Soreghan, G. S., Soreghan, M. J., & Hamilton, M. A. (2008). Origin and significance of loess in late Paleozoic western Pangaea: A record of tropical cold?. *Palaeogeography, Palaeoclimatology, Palaeoecology*, 268(3-4), 234-259. https://doi.org/10.1016/j.palaeo.2008.03.050

Soreghan, G. S., Sweet, D. E., & Heavens, N. G. (2014). Upland glaciation in tropical Pangaea: Geologic evidence and implications for late Paleozoic climate modeling. *The Journal of Geology*, 122(2), 137-163. https://doi.org/10.1086/675255

Struve, T., Pahnke, K., Lamy, F., Wengler, M., Böning, P., & Winckler, G. (2020). A circumpolar dust conveyor in the glacial Southern Ocean. *Nature communications*, 11(1), 1-11. https://doi.org/10.1038/s41467-020-18858-y

Sugden, D. E., McCulloch, R. D., Bory, A. J. M., & Hein, A. S. (2009). Influence of Patagonian glaciers on Antarctic dust deposition during the last glacial period. *Nature Geoscience*, 2(4), 281-285. https://doi.org/10.1038/s41467-020-18858-y

Sun, D., Bloemendal, J., Rea, D. K., An, Z., Vandenberghe, J., Lu, H., ... & Liu, T. (2004). Bimodal grain-size distribution of Chinese loess, and its palaeoclimatic implications. *Catena*, 55(3), 325-340. https://doi.org/10.1016/S0341-8162(03)00109-7

Sylvestre, F., Servant, M., Servant-Vildary, S., Causse, C., Fournier, M., & Ybert, J. (1999). Lake-Level Chronology on the Southern Bolivian Altiplano (18°–23°S) During Late-Glacial Time and the Early Holocene. *Quaternary Research*, 51(1), 54-66. doi:10.1006/qres.1998.2017

Teruggi, M. E. (1957). The nature and origin of Argentine loess. *Journal of Sedimentary Research*, 27(3), 322-332. https://doi.org/10.1306/74D706DC-2B21-11D7-8648000102C1865D

Timmermann, A., Jin, F. F., & Collins, M. (2004). Intensification of the annual cycle in the tropical Pacific due to greenhouse warming. Geophysical Research Letters, 31(12).
Todt, W., Cliff, R.A., Hanser, A. and Hofmann, A.W. (1996) in: Geophys. Monogr. 95, 429-437, *American Geophys*. Union https://doi.org/10.1029/2004GL019442

Toggweiler, J. R., Russell, J. L., & Carson, S. R. (2006). Midlatitude westerlies, atmospheric CO2, and climate change during the ice ages. *Paleoceanography*, 21(2). https://doi.org/10.1029/2004GL019442

Tonni, E. P., Nabel, P., Cione, A. L., Etchichury, M., Tófalo, R., Yané, G. S., … & Vargas, D. (1999). The 46nsenada and buenos aires formations (Pleistocene) in a quarry near la plata, Argentina. *Journal of South American Earth Sciences*, 12(3), 273-291. https://doi.org/10.1016/S0895-9811(99)00021-8

Torre, G., Gaiero, D. M., Sawakuchi, A. O., del Río, I., & Coppo, R. (2019). Revisiting the chronology and environmental conditions for the accretion of late Pleistocene-early Holocene Pampean loess (Argentina). *Quaternary Science Reviews*, 213, 105-119. https://doi.org/10.1016/j.quascirev.2019.04.018

Torre, G., Gaiero, D. M., Cosentino, N. J., Coppo, R., & Oliveira-Sawakuchi, A. (2020a). New insights on sources contributing dust to the loess record of the western edge of the Pampean Plain during the transition from the late MIS 2 to the early Holocene. *The Holocene*, 30(4), 537-545. https://doi.org/10.1177%2F0959683619875187

Torre, G., Gaiero, D. M., Cosentino, N. J., & Coppo, R. (2020b). The paleoclimatic message from the polymodal grain-size distribution of late Pleistocene-early Holocene Pampean loess (Argentina). *Aeolian Research*, 42, 100563. https://doi.org/10.1016/j.aeolia.2019.100563

Tripaldi, A., Zárate, M., Brook, G., & Li, G. (2011). Late Quaternary paleoenvironments and paleoclimatic conditions in the distal Andean piedmont, southern Mendoza, Argentina. *Quaternary Research*, 76(2), 253-263. doi:10.1016/j.yqres.2011.06.008

Tudhope, A. W., Chilcott, C. P., McCulloch, M. T., Cook, E. R., Chappell, J., Ellam, R. M., … & Shimmield, G. B. (2001). Variability in the El Niño-Southern Oscillation through a glacial-interglacial cycle. *Science*, 291(5508), 1511-1517. https://doi.org/10.1126/science.1057969

Unruh, A. L. (2001, November). Lead isotopic signatures of Cenozoic eolian deposits and implications for atmospheric circulation over Central Asia. In *Abstr. Prog. Geol. Soc. Am* (Vol. 33, p. 222). https://doi.org/10.1126/science.1057969

Vargas, G., Rutllant, J., & Ortlieb, L. (2006). ENSO tropical–extratropical climate teleconnections and mechanisms for Holocene debris flows along the hyperarid coast of western South America (17–24 S). Earth and Planetary Science Letters, 249(3-4), 467-483. https://doi.org/10.1029/2006GL028812

Walter, H. J., Hegner, E., Diekmann, B., & Kuhn, G. (2000). Provenance and transport of terrigenous sediment in the South Atlantic Ocean and their relations to glacial and interglacial cycles: Nd and Sr isotopic evidence. *Geochimica et Cosmochimica Acta*, 64(22), 3813-3827. https://doi.org/10.1016/S0016-7037(00)00476-2

Watson, A. J., Vallis, G. K., & Nikurashin, M. (2015). Southern Ocean buoyancy forcing of ocean ventilation and glacial atmospheric CO 2. *Nature Geoscience*, 8(11), 861-864. https://doi.org/10.1038/ngeo2538

Weltje, G. J. (1997). End-member modeling of compositional data: Numerical-statistical algorithms for solving the explicit mixing problem. *Mathematical Geology*, 29(4), 503-549. https://doi.org/10.1007/BF02775085

Wronkiewicz, D. J., & Condie, K. C. (1987). Geochemistry of Archean shales from the Witwatersrand Supergroup, South Africa: source-area weathering and provenance. *Geochimica et Cosmochimica Acta*, 51(9), 2401-2416. https://doi.org/10.1016/0016-7037(87)90293-6

Yang, J. H., Chung, S. L., Wilde, S. A., Wu, F. Y., Chu, M. F., Lo, C. H., & Fan, H. R. (2005). Petrogenesis of post-orogenic syenites in the Sulu Orogenic Belt, East China: geochronological, geochemical and Nd–Sr isotopic evidence. *Chemical Geology*, 214(1-2), 99-125. https://doi.org/10.1016/j.chemgeo.2004.08.053

Yokoo, Y., Nakano, T., Nishikawa, M., & Quan, H. (2004). Mineralogical variation of Sr–Nd isotopic and elemental compositions in loess and desert sand from the central Loess Plateau in China as a provenance tracer of wet and dry deposition in the northwestern Pacific. *Chemical Geology*, 204(1-2), 45-62. https://doi.org/10.1016/j.chemgeo.2003.11.004

Yuan, X., Kaplan, M. R., & Cane, M. A. (2018). The interconnected global climate system—A review of tropical–polar teleconnections. *Journal of Climate*, 31(15), 5765-5792. https://doi.org/10.1175/JCLI-D-16-0637.1

Zárate, M. A. (2003). Loess of southern south America. *Quaternary Science Reviews*, 22(18-19), 1987-2006. https://doi.org/10.1016/S0277-3791(03)00165-3

Zárate, M. A., Kemp, R. A., & Blasi, A. M. (2002). Identification and differentiation of Pleistocene paleosols in the northern Pampas of Buenos Aires, Argentina. *Journal of South American Earth Sciences*, 15(3), 303-313. https://doi.org/10.1016/S0895-9811(02)00041-X

Zárate, M., Kemp, R., & Toms, P. (2009). Late Quaternary landscape reconstruction and geochronology in the northern Pampas of Buenos Aires province, Argentina. *Journal of South American Earth Sciences*, 27(1), 88-99. https://doi.org/10.1016/j.jsames.2008.10.001

Zárate, M. A., & Tripaldi, A. (2012). The aeolian system of central Argentina. *Aeolian research*, 3(4), 401-417. https://doi.org/10.1016/j.aeolia.2011.08.002

Zech, W., Zech, M., Zech, R., Peinemann, N., Morrás, H. J. M., Moretti, L., ... & Glaser, B. (2009). Late Quaternary palaeosol records from subtropical (38 S) to tropical (16 S) South America and palaeoclimatic implications. *Quaternary International*, 196(1-2), 107 120. https://doi.org/10.1016/j.quaint.2008.01.005

Zech, M., Zech, R., Morrás, H., Moretti, L., Glaser, B., & Zech, W. (2009). Late Quaternary environmental changes in Misiones, subtropical NE Argentina, deduced from multi-proxy geochemical analyses in a palaeosol-sediment sequence. *Quaternary International*, 196(1-2), 121-136. https://doi.org/10.1016/j.quaint.2008.06.006

Zech, Jana., Terrizzano, Carla M., Garcia Morabito, Ezequiel., Veit, H. & Zech, Roland (2017). iming and extent of late pleistocene glaciation in the arid central andes of Argentina and Chile (22°-41°s). Universidad de La Rioja; *Cuadernos de Investigacion Geografica*; 43; 2; 697-718. http://dx.doi.org/10.18172/cig.3235